Renewable Energy 167 (2021) 1–19

Contents lists available at ScienceDirect

Renewable Energy

journal homepage: www.elsevier.com/locate/renene

Identifying key locations for shallow geothermal use in Vienna

Carolin Tissen [a, *], Kathrin Menberg [a], Susanne A. Benz [b], Peter Bayer [c], Cornelia Steiner [d], Gregor Götzl [d], Philipp Blum [a]

[a] Karlsruhe Institute of Technology (KIT), Institute of Applied Geosciences (AGW), Kaiserstraße 12, Karlsruhe, Germany
[b] University of California San Diego (UCSD), School of Global Policy and Strategy (GPS), 9500 Gilman Drive, CA, 92093-0519, USA
[c] Martin Luther University Halle, Faculty of Geosciences, von-Seckendorff-Platz 3, 06120, Halle/Saale, Germany
[d] Geological Survey of Austria, Department of Hydrogeology and Geothermal Energy, Neulinggasse 38, 1030, Wien, Austria

ARTICLE INFO

Article history:
Received 23 April 2020
Received in revised form
23 September 2020
Accepted 6 November 2020
Available online 11 November 2020

Keywords:
Geothermal potential
Groundwater heat pump (GWHP)
Borehole heat exchanger (BHE)
Heat supply
Subsurface urban heat island (SUHI)
Geographic information system (GIS)

ABSTRACT

Decarbonising the heating sector is crucial for reducing CO_2 emissions. This is in particular true for Central European cities such as Vienna, where 28% of the total CO_2 emissions are caused by the energy supply for buildings. One promising option for environmental friendly heat supply is the use of shallow geothermal energy. To determine whether shallow geothermal systems are a feasible option to meet the urban heating demand, the Python tool GeoEnPy is developed and applied to a case study in Vienna. It allows the evaluation of the anthropogenic heat input into the subsurface, the theoretical sustainable potential, the technical geothermal potential, and the heat supply rate. The overall heat flow in Vienna is 17.6 PJ/a, which represents 38% of the current heating demand or indeed 99% once all buildings are thermally refurbished. The technical geothermal potential can satisfy the current heating demand for 63% (BHE system) or rather 8% (GWHP system) of the city area. GeoEnPy reveals that BHE systems are most feasible in the eastern and southern districts of Vienna. Our findings can guide integration of shallow geothermal use in spatial energy management focused on key locations to supply buildings with decentralised and sustainable heat from the subsurface.

1. Introduction

Ambitious goals and concepts to encourage application of renewable energy technologies and to reduce CO_2 emissions, especially in the heating sector, exist on EU- [1], country- [2] and city-level [3,4]. From 1995 to 2016, Vienna's heating sector moved away from fossil fuels (oil −44%, coal −99%, gas −8%) towards more renewable energy resources (+34%). Despite this progress, the building energy supply still causes 28% of CO_2 emissions [5]. Shallow geothermal systems are one of the key technologies to replace fossil fuels, reduce CO_2 emissions and achieve low carbon cities [6–9]. They are a particularly good option for areas or districts with a low heat demand density, for which a connection to a district heating (DH) network is not economically and/or environmentally efficient [10,11]. Currently, 1070 closed- and 762 open-loop geothermal systems are already installed in Vienna, and an increased contribution from geothermal sources is anticipated, especially in city parts without a DH system and where new buildings are planned [12].

Closed- or open-loop geothermal systems extract the energy stored in the shallow subsurface. Closed-loop systems use borehole heat exchangers (BHE) to harness heat from the ground. Open-loop systems, known as groundwater heat pumps (GWHP), extract water from the aquifer, gain the thermal energy with a heat transfer system and re-inject the cooled water back into the aquifer [13]. Thorough planning is crucial for the development of economically feasible systems that are optimised according to their hydro- and geological conditions. Numerous studies explored and estimated the feasibility of geothermal use in urban areas with various approaches [14–18]. The basic concept of linking the energy available in the ground with the heat that can be used is a definition of a geothermal potential.

Bayer et al. [19] define the maximum amount of energy stored in the ground as theoretical potential and the amount of energy that can be extracted by a specific geothermal system as technical potential. Estimations of the geothermal potential for both, open and closed-loop systems, were done in various ways, using energy balance calculations, analytical or numerical models, and

* Corresponding author.
E-mail address: carolin.tissen@kit.edu (C. Tissen).

https://doi.org/10.1016/j.renene.2020.11.024
0960-1481/

geographic information systems (GIS). GIS offers a comfortable way to process, analyse and combine spatial hydro-/geological data, and to display the final results as easily accessible geothermal potential maps [e.g. 20,17,18,21,22].

Much attention was so far given to the sustainability and long-term effects of geothermal energy. Intensive use or a high system density can lead to interference [23–26]. Furthermore, decreasing ground temperatures can lead to a decrease in efficiency over time, which in turn can cause conflicts amongst different geothermal users [e.g. 27,28,29]. To maintain system efficiency and to avoid overly cooling of the subsurface, some recent studies propose coupling of solar panels and ground source heat pump (GSHP) systems [30,31]. Another factor that enhances sustainable use is the natural replenishment of thermally-used ground, which is substantially augmented by passive anthropogenic heat input into the urban subsurface [32–35]. The heat input from buildings, increased ground surface temperature (GST) and subsurface infrastructures, such as district heating (DH) pipes and sewers, was studied in several cities [e.g. 36,37,38,39]. These heat sources also lead to increased groundwater temperatures (GWT) in urban aquifers. This phenomenon of urban ground and groundwater warming, which is observed globally on city-scale, is called subsurface urban heat island (SUHI) effect [e.g. 40,41,42,43,44]. Menberg et al. [45] and Benz et al. [46] developed a 1D analytical and statistical heat flux model to estimate the mean annual heat flux and flow from anthropogenic heat sources.

Although several studies relate the anthropogenic heat input to the heating demand [32–34,47,48], the majority of studies focus either on geothermal potential on district- [49–51] or city-scale [14,15,52], or on quantifying the anthropogenic heat input into the subsurface [45,53]. Thus, so far there is little known about the role of enhanced heat fluxes into the urban ground for the technical performance and the sustainable operation of geothermal systems on city-scale.

The objective of this study is to compute, spatially resolve and combine the technical geothermal potential of open- and closed-loop systems with the annual anthropogenic heat input. By relating the technical geothermal potential to the heating demand, this study identifies key locations for shallow geothermal use in Vienna. The quantity used to assess the technical potential is the technically feasible heat supply rate, which considers the available space for system installation, as well as site-specific hydro-/geological conditions. Furthermore, the subsurface heat fluxes from seven different anthropogenic heat sources are calculated and contrasted to the local heat demand to estimate the sustainable potential. For this procedure, the Python based tool GeoEnPy is developed and applied.

2. Materials and methods

2.1. Study site

Vienna, the capital of Austria, consists of 23 districts with a total size of 415 km^2 (Fig. 1) and is located at the easternmost extension of the Alps and at the western margin of the Vienna Basin. Hydrogeological areas with their distinct groundwater conditions are oriented parallel to the river Danube, which splits the city into an eastern and western part. From the Danube floodplains in the east to the Wienerwald in the west, so from the younger to the older strata, the following four hydrogeological zones can be distinguished: Holocene and Pleistocene gravel units, Miocene unconsolidated sediments of the Vienna Basin, and Alpine bedrock (Figure C.14). The Holocene gravel units of the Danube plain form a continuous, porous aquifer with a high permeability and an average thickness of 7–14 m [54]. The gravel units at the bed valleys of Wienerwald consist of platy and loamy sandstone gravels and therefore are less permeable and less productive. Here, the groundwater flow direction is parallel to the local streams. The Pleistocene terraces only have moderate to low abundancy of groundwater and the groundwater flow direction is from west to east. The Miocene sediments of the Vienna Basin are composed of silts, clays and fine sands and form local, unconfined aquifers with a moderate yield. The Alpine bedrock in the western part comprises the fractured aquifer of the Flysch zone and the karst aquifer of the calcareous Alps [55,56].

2.2. Input data

The data used for anthropogenic heat flux, heat flow and heat supply rate computations include point, line, areal, as well as raster data. To unify the different data for the computation and to avoid yearly or seasonal temperature bias, data were averaged over one year or, where possible, 10 year means (2007–2016) were applied.

The maps of the district heating (DH) network, subway temperature and the heating demand are confidential and the Geological Survey of Austria (GBA) only shared them as Web Feature Service (WFS) for this study. All further data bases are freely accessible via the online open data portal of Vienna ([57], Table D.5).

Temperature data from basements, underground carparks and subway tunnels as well as groundwater temperature (GWT) and groundwater (GW) level data are available as point features from 66 or rather 315 wells inside and outside of Vienna (Fig. 1). Monthly mean GWT and GW level data are freely available [58]. Most monitoring wells are equipped with data loggers and record GWT and GW level data four times an hour [59]. Air temperature data in basements (57 locations) and underground carparks (12 locations) were recorded for one annual cycle using iButtons (Figure C.15). Air temperatures within subway tunnels were recorded for 38 locations by Wiener Linien [60].

Line data include sewers, subway tunnels, and DH pipes. Most of the sewage network is operated as a mixed system; that is grey water and rainwater are discharged together [61]. The total length is about 2500 km and the available spatial data also includes information about the vertical dimensions of the sewers. Consequently, the exact diameter and vertical position of each sewer segment is known. The total length of the subway system running below ground is around 46 km. The district heating network is split into a primary and secondary network with different pressures and temperatures. This network has a total length of approx. 1230 km and supplies over 30% of Vienna's households with energy for heating and domestic hot water [62,63].

Areal data comprises WFSs, shapefiles and raster datasets. The heating demand (HD) was provided as a WFS in form of hexagonal polygons of 8657 m^2 each. The assessment of the HD involves the present and future heating demand, both expressed in MWh per year and hexagon. The heating demand of the present building stock was determined based on the construction period, building height, building use, gross floor area and heating degree days. The future heating demand refers to the OIB-RL6 standards and assumes that all buildings are thermally refurbished [64]. A detailed description of the heating demand assessment is given by Ref. [65]. Daily air temperature measurements were collected and interpolated by the Central Institute for Meteorology and Geodynamics [66]. The interpolation explicitly takes into account the topographical characterization of the measurement location. The GBA supplied average air temperatures from 2006 to 2016 as WFS with a spatial resolution of 1 km by 1 km. By combining air temperature with an offset depending on the surface material, the ground surface temperature (GST) is estimated [46]. The different offsets for

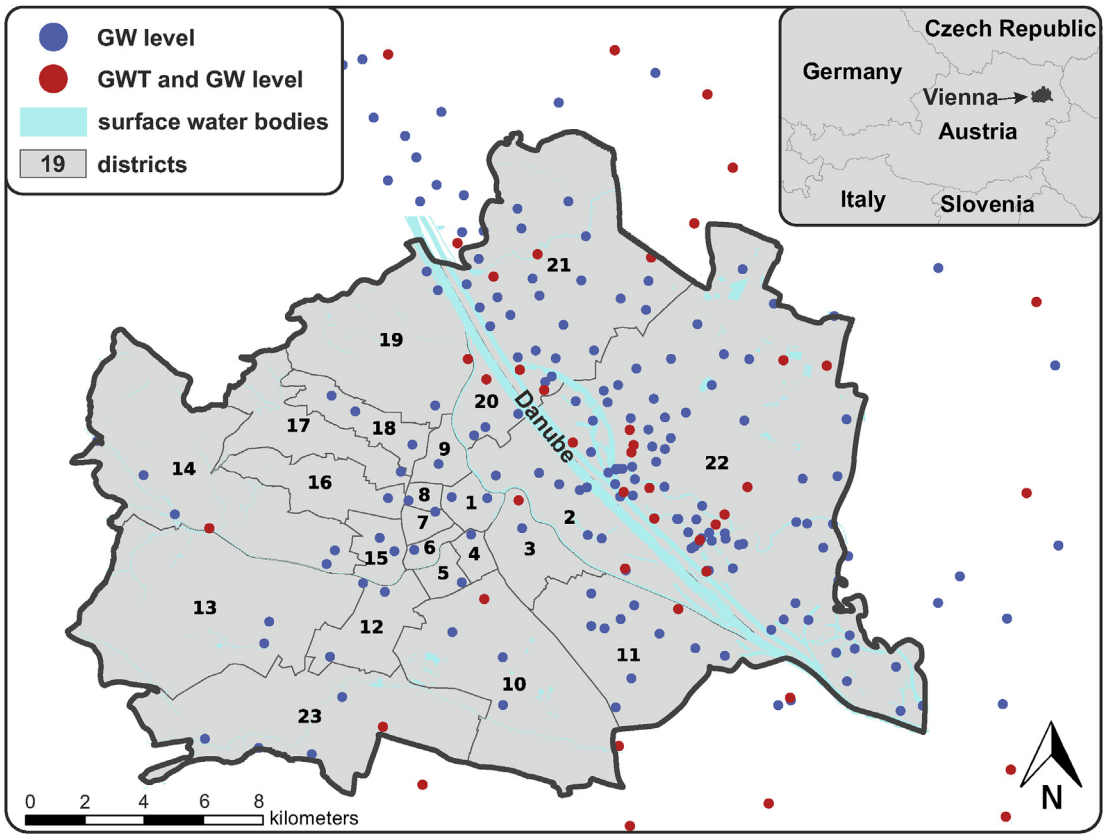

Fig. 1. Location of Vienna, its 23 urban districts and measuring sites for groundwater temperature (GWT) and groundwater level (GW level).

grass, asphalt, bare soil and sand were determined by Dědeček et al. [67] and adapted to the land use categories described in the Urban Atlas [68]. Continuous and discontinuous urban fabric make up 27% of Vienna's land use, whereas 22% are covered by green urban areas and forest. The distribution of Vienna's land use categories and the matching temperature offsets according to Dědeček et al. [67] are summarised in Table D.6.

Further areal data in the form of shapefiles are building and tunnel footprints, surface water, hydro- and geological data, as well as geothermal potential maps. The geothermal potential maps of borehole heat exchangers (BHE) and groundwater heat pumps (GWHP) give an overview on attractive locations by pointing out whether and for which type of use a location is suitable. A detailed description of the assessment for both geothermal potential maps can be found in Götzl et al. [69]. About 30% of the city area of Vienna are ideally suited for the use of shallow geothermal energy. Especially east of the Danube River, for example in the rapidly growing districts 21 and 22, one can expect high yields from thermal groundwater use. The potential maps for BHEs do not show an actual power potential in form of an amount of energy per area and time unit, but rather express the potential as thermal conductivity (in W/m/K) for different depth layers. The potential map of the geothermal use of groundwater displays the maximum thermal power of a single well system. Within each of the 14 hydrologically homogeneous areas, the thermal potential primarily reflects the hydraulically effective thickness of the aquifers. The estimated well performance to assess the thermal power is based on the assumption of a maximum cooling or warming of the extracted groundwater by 5 K and considers only the top groundwater body.

The digital elevation model (DEM) is available as a raster data file with a resolution of 1 m × 1 m. Additional data, such as sewage water temperature or heat loss rate of the DH system, as well as all input layers with their type, value, unit and source are listed in Table D.5.

2.3. Methods

2.3.1. Calculation of the anthropogenic heat flux and flow

The simulation of the vertical anthropogenic heat fluxes into the unsaturated zone is based on the method described by Benz et al. [46]. The heat flux q and heat flow Q calculation is accomplished on a regular grid with a 25 m by 25 m grid cell size, and comprises five steps (Fig. 2). The spatial analysis of all five steps is implemented in the Python tool GeoEnPy. GeoEnPy applies Python with the site package ArcPy to trigger and run functions from the ArcGIS toolbox. It was specifically developed for this study to evaluate the average annual anthropogenic heat input and shallow geothermal potential of Vienna's subsurface. It can be applied to other cities as long as basic data such as groundwater temperature, groundwater level, information about surface material and building footprints are available. The first two steps prepare the input data, and steps three to five calculate the heat flux and flow.

In the first step, the GWT and GW level data from 2007 to 2016 are averaged and interpolated in ArcGIS using ordinary kriging. The resulting raster has a resolution of 25 m × 25 m (Figure C.16), which is consistent with the size of the grid layer. In the second step, all input layers are linked to one another and combined in different compositions according to the seven individual heat sources. These combined layers are the basis for the anthropogenic heat flux q and

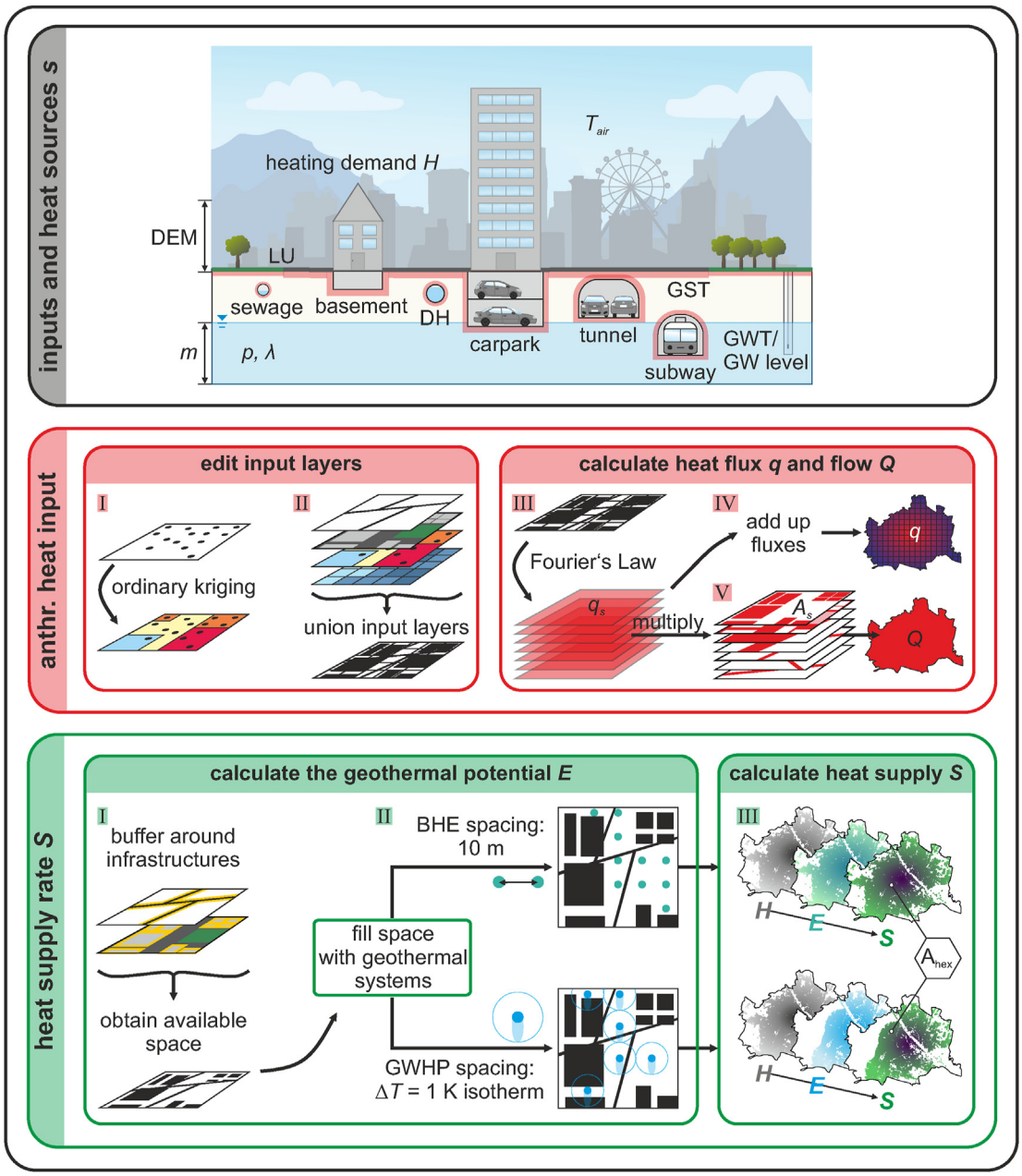

Fig. 2. Workflow of the calculation of the heat flux and the heat supply rate including the anthropogenic heat flux model with its input data and anthropogenic heat sources. List of used abbreviations: hexagon area (A_{hex} = 8657 m^2), area of the anthropogenic heat source (A_s), digital elevation model (DEM), district heating (DH), temperature difference (ΔT), technical geothermal potential (E), ground surface temperature (GST), groundwater (GW), groundwater temperature (GWT), heating demand (H), thermal conductivity (λ), land use (LU), aquifer thickness (m), porosity (p), total heat flux (q), heat flux per heat source (q_s), heat flow (Q), heat supply rate (S) and air temperature (T_{air}).

heat flow Q calculation in the third step. The anthropogenic heat flux q represents the conductive heat transport from the heat source to the groundwater surface and is described by Fourier's Law: $|q| = \lambda \cdot \Delta T/\Delta d$, where λ is the thermal conductivity, ΔT is the difference in temperature and Δd the distance between two points. As shown in Eq. (1), Fourier's Law is adapted to each heat source except for the DH system. Advective heat transport is not considered in this study, since there are no data available for leakage rates of the sewage or district heating network.

$$q_s^g = (\lambda^g + \delta\lambda) \cdot \frac{T_s - (T_{GW}^g + \delta T_{GW})}{(d_{GW}^g + \delta d_{GW}) - d_s^g} \quad (1)$$

The resulting q_s^g represents the average heat flux as energy per square meter per grid cell g and heat source s. T_s is the respective temperature of the heat source s, T_{GW}^g is the GWT, λ^g is the thermal conductivity and d_{GW}^g as well as d_s^g the depth of the groundwater table and the heat source in the specific grid cell g. In order to

account for spatial variability, Eq. (1) is evaluated for the respective heat source s and within each grid cell g. In order to account for uncertainty in terms of measurement accuracy and parameter uncertainty, a Monte Carlo simulation is carried out. For this, Eq. (1) is evaluated over 1000 iterations, where $\delta\lambda$, δT_{GW} and δd_{GW} reflect the uncertainties of the thermal conductivity, GWT and GW level. The anthropogenic heat flux from the DH network considers the percentage of downward directed heat flux P and the heat loss rate L for the primary and secondary DH pipes with a diameter D_{DH}:

$$q_{DH}^{g} = \frac{L \cdot P}{D_{DH}} \tag{2}$$

Eq. (2) is applied for each grid cell g having an intersection with a DH pipe.

In the fourth step, the individual heat fluxes from each heat source are added up to obtain the total heat flux $q_{tot} = \sum q_s^g \cdot \frac{A_s}{A_g}$ per grid cell. Here, A_s and A_g are the areas of the heat source and grid cell, respectively.

In the last step, the heat flow Q of the entire city area of Vienna is calculated. For this, the heat flux q_s^g Eq. (1) and (2) are multiplied with the source area. The sum of these products gives the total vertical ground heat flow of Vienna for the anthropogenic heat sources considered and expressed in PJ/a.

2.3.2. Calculation of the technical geothermal potential and heat supply rate

The following procedure for estimating the technical geothermal potential and the heat supply rate is in line with the evaluation steps described by Tissen et al. [49]. However, for the present study of Vienna, no data for domestic hot water demand is available, so the heat supply rate S is defined as ratio of the technical geothermal potential E to space heating demand H. The technical geothermal potential is evaluated in several steps, before the heat supply rates for borehole heat exchanger (S_{BHE}, S_{BHE_h}) and groundwater heat pump (S_{GWHP}) systems are calculated in an additional step.

To calculate heat supply rates for BHE systems (S_{BHE}, S_{BHE_h}), the geothermal potential, expressed as thermal conductivity [57], first has to be transformed into a specific standard q_{BHE} and raised q_{BHE_h} heat extraction rate. The transformation is conducted in two different ways. On the one hand, the Swiss Norm SIA 384/6 [70] is employed to deduce the standard heat extraction rate q_{BHE} for a thermal conductivity value. On the other hand, higher heat extraction rates q_{BHE_h} due to groundwater flow are considered and the specific heat extraction rates by VDI 4640 part 2 [71] are applied for the individual rock types of the aquifers.

The first step of the evaluation is a spatial analysis that yields the available space for the installation of BHE and GWHP systems. Here, a buffer of 2 m is placed around each building, tunnel and underground carpark, as well as a smaller buffer of 1 m around each subsurface supply pipe [72]. The buffer zones are merged and subtracted from the total city area to obtain the available space for geothermal system installation.

In a second step, this available space is filled with BHE and GWHP systems considering technology-specific spacings. In case of BHEs, the spacing is 10 m (best practice by GBA). In case of GWHP systems, the well space is defined as maximum extension of the thermal plume for a temperature reduction ΔT by 1 K. A detailed description of the plume evaluation is given by Tissen et al. [49]. Based on the input data listed in Table D.5, an $\Delta T = 1K$ isotherm for each hydrogeological unit is evaluated (Figure C.17). For simplicity, and because the heating demand is given per hexagon, the number of possible BHEs and GWHPs per grid cell g are summed up to obtain the maximum feasible number of system installations per hexagon h.

The product of the number of BHE n_{BHE}^{h}, a BHE length l of 150 m (best practice by GBA) and the average heat extraction rate q_{BHE}^{h} or q_{BHEh}^{h} yields the technical geothermal potential E_{BHE} or E_{BHE_h}. In contrast, E_{GWHP} is the product of the number of well pairs n_{GWHP}^{h} and the average GWHP potential q_{GWHP}^{h} per hexagon h.

In a third step, the heat supply rates S_{BHE}, S_{BHE_h} and S_{GWHP} are calculated for each hexagon h:

$$S_{BHE}^{h} = \frac{q_{BHE}^{h} \cdot l \cdot n_{BHE}^{h} \cdot t \cdot COP}{(COP-1) \cdot H^{h}} \cdot 100 \tag{3a}$$

$$S_{GWHP}^{h} = \frac{q_{GWHP}^{h} \cdot n_{GWHP}^{h} \cdot t \cdot COP}{(COP-1) \cdot H^{h}} \cdot 100 \tag{3b}$$

The heat supply rates [%] consider an operation time t of 1800 h/a and coefficient of performance (COP) of 4. The heat supply rates are evaluated for a heating demand H referring to the current building stock in the hexagon and for a future scenario in which all building have been thermally refurbished according to the OIB-RL6 standards of Austria [64].

Furthermore, the ratio between total annual heat flow Q and heating demand H is defined as theoretical sustainable potential.

3. Results and discussion

3.1. Anthropogenic heat flux

The computed anthropogenic heat flux (AHF) q of all seven individual heat sources and the total heat flux show a significant spatial variability (Figure C.18). The highest mean heat flux originates from underground carparks (15.38 ± 5.20 W/m^2) and DH systems (13.67 ± 1.91 W/m^2). Whereas the smallest positive median heat flux rate is caused by elevated GST (0.11 ± 0.01 W/m^2) and buildings (2.58 ± 2.15 W/m^2). Tunnels have a negative mean heat flux (−1.13 ± 0.09 W/m^2). However, these results are based on two tunnels with a length of just 2.1 km and 0.21 km, respectively, and efficient ventilation systems. Hence, it is assumed that the mean annual air temperature inside and outside of the tunnels are equal, and therefore cooler than the mean GWTs. Thus, tunnels act as heat sinks and cool the urban underground when multi-annual mean temperatures are used for assessment. Seasonal patterns might differ.

Benz et al. [32,46] also calculated the anthropogenic heat flux by applying Fourier's Law in the two German cities, Karlsruhe and Cologne, as well as in Osaka, Japan. In the German cities the DH system causes the highest AHF, with the mean heat flux by the DH system in Karlsruhe being four times larger than in Vienna. One reason for this difference is the generally low heat loss of Vienna's DH network, which is reported to be below the average heat loss rate of European DH networks [73]. The mean heat flux by buildings in Vienna is in good accordance with the results for Karlsruhe (3.61 ± 3.37 W/m^2), yet higher than in Cologne (0.57 ± 0.25 W/m^2) and

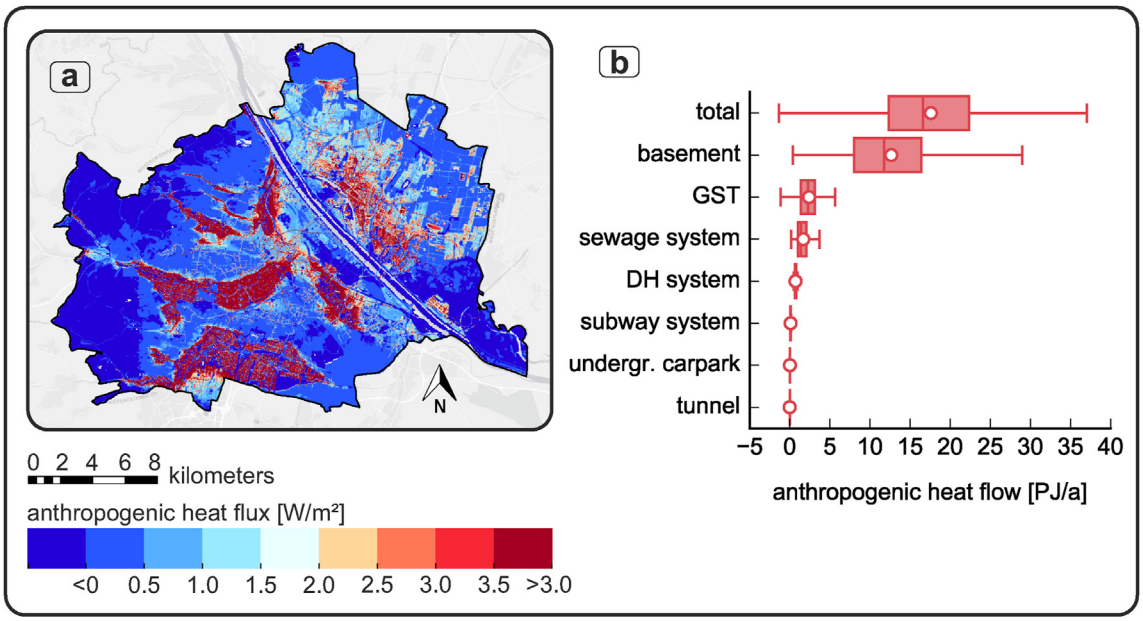

Fig. 3. Map of the total average anthropogenic heat flux q per grid (25 m by 25 m resolution) (a) and boxplots of the total and individual anthropogenic heat flows Q (b). Mean values are indicated by a white dot.

Osaka (0.32 ± 0.18 W/m^2). In contrast, relatively high heat fluxes of 5.9–8.0 W/m^2 are reported for buildings in Basel, Switzerland [33]. This wide range of heat flux values from buildings in different cities is mainly due to differences in ground thermal conductivity, groundwater flow velocity, insulation and temperatures in buildings, and whether basements are within the un- or saturated zone [32,33,74,75].

The sum of all seven AHFs per grid cell, the total heat flux, is displayed in Fig. 3a. In general, areas with shallower groundwater (GW) have a higher AHF. The shallowest depth to water table is along the Danube River and the old Danubian channel, as well as close to small streams in the north-western parts (Fig. 1). Here the total heat flux is above 3 W/m^2. Moreover, GST also significantly influences the total heat flux (Figure C.19). In green urban areas and forests (Wiener Wald) the total heat flux is negative, with GWT being higher than GST, and thus the groundwater releases heat towards the ground surface. In contrast, regions with sealed surfaces and a high building density in continuous and discontinuous urban fabrics represent areas of a high total (downward) heat flux.

The mean total heat flux per pixel is 5.22 ± 0.82 W/m^2. The mean heat flux per pixel without underground carparks, tunnels and subway system is 1.07 ± 0.32 W/m^2, which is in good accordance with the mean heat flux per pixel in Karlsruhe with 1.10 ± 0.73 W/m^2 [46]. A main reason for this is that the average groundwater depth below the surface in Vienna (6.2 m) is similar to the one given for Karlsruhe (5.4 m). In contrast, for the city of Cologne, where the mean water table is around 10 m below surface, the total heat flux is only 0.39 ± 0.12 W/m^2.

Locally, underground carparks and subway tunnels have the largest anthropogenic heat impact, yet on city scale the bulk contribution of these features is smallest. The highest heat flow over the entire city area arises from buildings (12.65 ± 6.45 PJ/a) and increased GST (2.41 ± 1.21 PJ/a), whereas the lowest heat flow originates from underground carparks (0.02 ± 0.01 PJ/a) and tunnels (−4.48 ± 0.36 TJ/a) (Fig. 3b). The high standard deviations of the total heat flow values here reflect the interplay of parameter uncertainty in the calculation of the heat flows and the spatial variability over the study area (Figure C.18, C.19). Buildings and

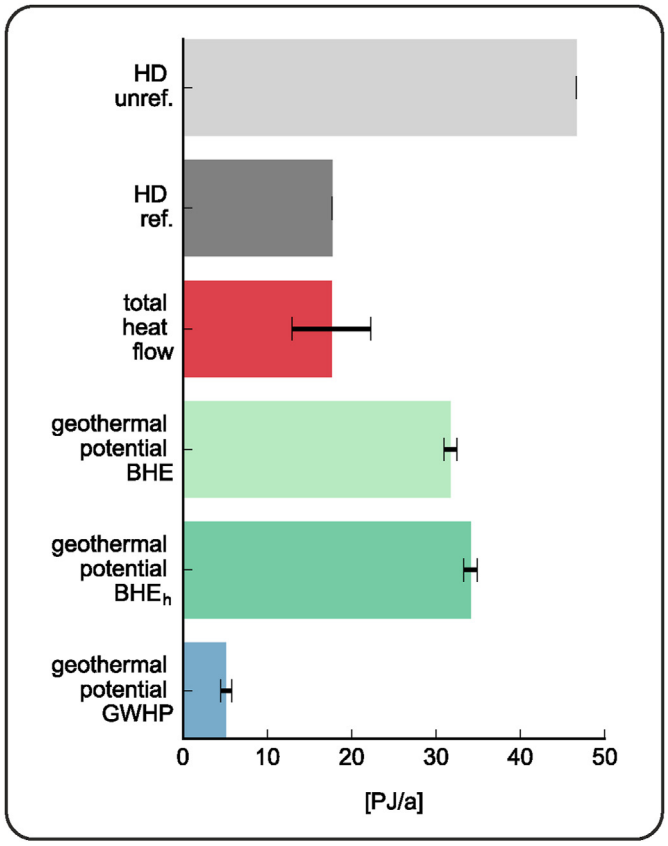

Fig. 4. Comparison of the current (unref.) and future (ref.) heating demand (HD) with the total mean anthropogenic heat flow and the mean technical geothermal potentials of borehole heat exchanger with standard (BHE) and higher (BHE$_h$) heat extraction rate, and groundwater heat pump (GWHP) systems. Uncertainties are given as standard deviation, except for the heating demand for which no uncertainty is given.

sealed ground cover 14% and 82% of the area of Vienna, whereas the twelve underground carparks and the two tunnels only account for 0.01% and 0.03% of Vienna's area, respectively. Consequently, the diffuse heat input in cities not only depends on the heat flux and its governing factors (such as basement depth and temperature), but on the large scale mainly on the size of the heat source. Menberg et al. [76] and [Benz et al. 46, 32] also identified buildings and increased GST as main contributors to the annual ground heat flow and heat anomalies beneath Karlsruhe, Cologne and Osaka.

3.2. Sustainable and technical geothermal potential

The calculated anthropogenic heat flow indicates a continuous heat input into the subsurface throughout the year. In principle, this means that an annual amount of 17.6 ± 6.99 PJ/a can be used by geothermal technologies to sustainably satisfy Vienna's heating demand. Considering a steady-state system and neglecting the impact of increasing heat flow in case of decreasing GWT, on average 37.7% of the current heating demand, and actually 99.5% of the future heating demand (in case of thermally refurbished buildings) could be supplied sustainably (Fig. 4). Differing values for the sustainable potential, expressed as the ratio between available energy from heat flow Q to heating demand H, were reported by [Benz et al. 46, 32] for Karlsruhe (32%) and Cologne (9%) in Germany, and smaller rates between 3% and 5% in Osaka, Japan. The sustainable potential as it is computed here gives an indication of how much heat is annually recharged from the surface and could be utilized theoretically. However, it includes neither the presently stored heat, nor the additional geothermal heat flux from below, which are both part of the sustainably extractable energy. The computed values here can therefore be considered as a lower boundary of the full sustainable potential. Moreover, they are also conservative estimates, as ground heat extraction enhances the heat flux towards cooled ground regions. Finally, sustainable heat extraction rates could be also increased by recharging the ground in the summer season using heat release from geothermal cooling systems or waste heat.

Considering the thermal energy stored in the Quaternary aquifer [48], a GWT reduction of 5 K would yield an amount of thermal energy that is 1.2 and 3.1 times larger than the respective heating demands.

In contrast, the technical geothermal potential of all GWHP systems operating for 1800 h/a is ten times smaller than the theoretical geothermal potential. Due to the large system spacing of 25 m–176 m, the total number of GWHP is limited and consequently, only a small fraction of the stored energy can be harnessed by GWHPs each year. In total, solely 11% and 29% of the heating demand before and after refurbishment can be satisfied by GWHP systems.

The technical geothermal potential of BHE applications on the other hand shows more promising results. A higher heat extraction rate (scenario BHE_h) even increases the potential by further 7.6%. After refurbishment the geothermal potential exceeds the heating demand by a factor of two. Thus, in the current state 68% of Vienna's heating demand could be supplied by BHE. BHEs are assumed to be installed with a much higher density of systems than GWHP and thus the vertical ground heat flux can be exploited more efficiently. However, in reality adjacent BHEs may interfere and thus compromise the efficiency of heat extraction [47,77]. Yet, the current approach does not consider the efficiency of the geothermal technologies due to lack of data. Also, BHEs utilize large volumes of the ground, as a depth of 150 m is assumed for the study case of Vienna. In comparison, GWHPs extract heat from typically layered aquifers of lower thickness and thus induce broader thermal anomalies [49,78].

Hence, the difference between theoretical and technical geothermal potential is just a matter of optimising the system spacing and technical method of energy extraction from the ground, while taking care of a sustainable management of this resource. Sustainability could be achieved if the annual anthropogenic heat input was recycled by BHE and/or GWHP applications. In fact, for 1.8% of the hexagons the anthropogenic heat flow is larger than the technical geothermal potential, and for 14% of the hexagons even larger than the heating demand of unrefurbished buildings.

3.3. Heat supply rate

The comparison of the technical geothermal potential and the heating demand leads to the heat supply rate. The average BHE heat supply rate per district is 12%–180% before and 35%–427% after refurbishment. So in 7 or rather 14 out of 23 districts the average BHE potential is higher than the average heating demand before or after refurbishment, respectively. The highest GWHP heat supply is located in the southern parts of district 10 and reaches 34% in case of unrefurbished and 83% in case of refurbished buildings (Fig. 5).

The BHE heat supply rate per hexagon is above 100% in 64% and 82% of all hexagons before and after refurbishment, respectively. Looking at these rates for the hexagons on district level, reveals that the outer districts 14, 21 and 22 are more likely to yield a heat supply rate above 100% than the inner-city districts 4, 7 and 8 (Fig. 5c). This spatial distribution of the BHE heat supply rates exhibits a radial pattern with increasing supply rates from the city centre towards the outer districts, illustrated by the heat supply map in Fig. 5a. The lower heat supply rates in the inner districts (1–9) are attributed to a larger gross floor area, higher population and building density, leading to less available space for system installations. Moreover, old buildings from the "Gründerzeit" epoch (19th century) in the city centre have a high heating demand. In contrast, in the outer districts (11, 14, 19, 21, 22, 23) with discontinuous urban fabric, heating demand is lower and also more space is available for geothermal systems. Dochev and Peters [79] also conclude in their study that the heat supply rate depends more on the heating demand, than on geological conditions. They also obtain similar values for the heat supply rate (below 75%) in central areas of the city of Hamburg, Germany. In their study on the theoretical geothermal potential of the city of Ludwigsburg, Germany, Schiel et al. [52] also pointed out that it is more likely to meet the heating demand in residential areas.

For 9% (unrefurbishment) and 22% (refurbishment) of all hexagons (Fig. 2), the GWHP supply is above 100%. In contrast to the pronounced radial distribution of the BHE heat supply rate, the GWHP supply rate shows no distinct spatial distribution (Fig. 5b). The likelihood of achieving a heat supply rate above 100% is higher in district 2, 10 and 11 in the south than in the inner and eastern district 7, 21 and 22 (Fig. 5c). As stated above, the GWHP potential, and so the heat supply rate (Fig. 5c), are mainly influenced by the GWHP spacing and the number of potential GWHP systems, as well as the hydrogeological conditions (Figure C.20). The aquifer east of the Danube River (district 21 and 22) is the most productive aquifer with the highest yield. Given the large extension of the induced thermal plumes, the spacing between the systems is large here

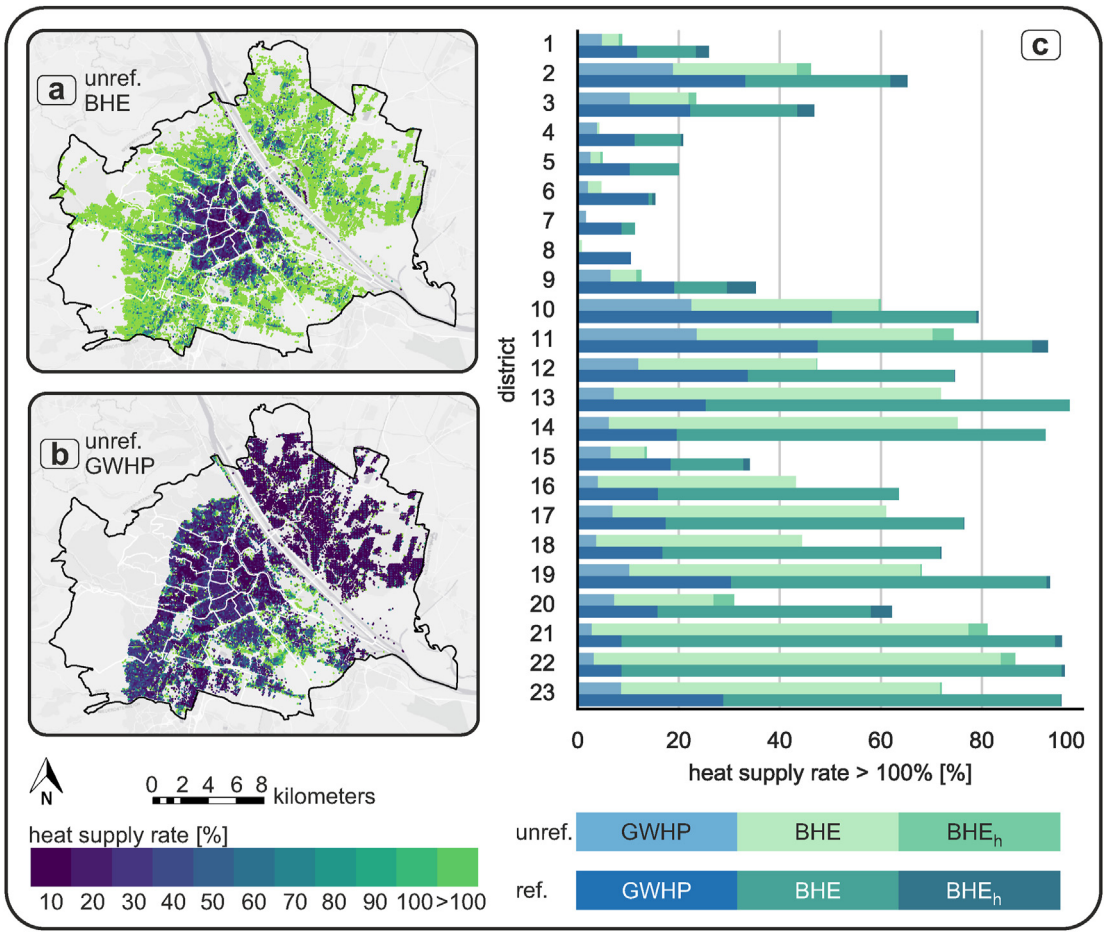

Fig. 5. The maps display the spatial distribution of the heat supply rate referring to the heating demand of unrefurbished (unref.) buildings for borehole heat exchanger (BHE) (a) and groundwater heat pump (GWHP) systems (b). The bar graph shows the percentage of hexagons with a heat supply rate above 100% for all 23 districts (Fig. 1) and a heating demand referring to un- (unref.) and refurbished (ref.) buildings (c). Scenario BHE$_h$ considers partly higher heat extraction rates due to groundwater flow.

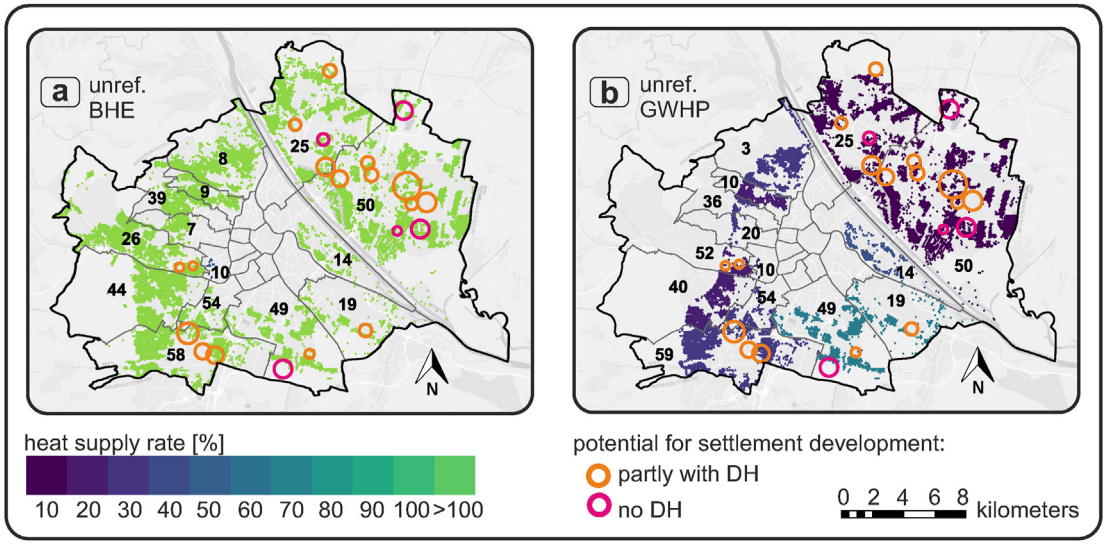

Fig. 6. Spatial distribution of the average heat supply rate per district for borehole heat exchangers (BHE) (a) and groundwater heat pumps (GWHP) (b) assuming that all buildings are thermally refurbished (ref.). The numbers within each district refer to the sustainable geothermal potential in percent. The circles indicate areas with potential for settlement development [81], where the district heating system (DH) is already partly expanded (orange) or no DH system (magenta) exists. Circle size represents the potential for settlement development (smallest circle: building design of 460 housing units, largest circle: building design of 9400 housing units. (For interpretation of the references to colour in this figure legend, the reader is referred to the Web version of this article.)

(176 m), and therefore, fewer installations are possible leading to the lowest total supply rate of Vienna. This finding appears to contradict the fact that this areas have the most productive aquifer, yet the extension of the thermal plume increases with groundwater flow velocity or pumping rate [78]. In future studies, the definition of GWHP spacing based on temperature plumes has to be reconsidered, so that the technical geothermal potential can be increased and approach the theoretical geothermal potential of the aquifer. For this purpose more GWT, ground water level and flow velocity data are required, especially west of the Danube River, to improve spatial interpolation and the estimation of temperature plumes. In addition, a numerical heat transport model could be developed to optimise the use of the groundwater.

3.4. Key locations for shallow geothermal use

Areas with a high heat supply rate as well as a high theoretical sustainable potential are the key locations for shallow geothermal use. Here, the heating demand could be met with BHE or GWHP systems. Additionally, the extracted energy is for a large part compensated by the anthropogenic heat input. Solely city blocks without district heating are considered for the identification of key locations, so that a competition with heat supply by district heating is avoided (Fig. 6). The DH network concentrates on the city centre, so that the DH-free areas are located in the outer districts, which conveniently also have the highest heat supply rates before refurbishment. Except for district 15, all districts show an average BHE heat supply rate above 100%. District 21 and 22 only have a GWHP supply rate of maximum 7%, however the southern parts of district 10 and 11 achieve a supply rate above 55%. The average sustainable potential per districts ranges between 8% and 58%. Epting et al. [80] compared the waste heat, defined as higher GWT due to the heat input by buildings and reinjection of cooling water, to the heating demand of Basel, Switzerland. They concluded that for 30% of the area the waste heat is sufficient to satisfy the heat demand. In Vienna, a sustainable potential above 100% is obtained for 15% of the area without a district heating system. After refurbishment or for newly constructed low-energy buildings, the heat supply rate and sustainable potentials are even more propitious. For a heating demand reduced by 62%, a heat supply rate above 100% is achievable for 97% (BHE) and 26% (GWHP) of the hexagons. Additionally, over one third of the hexagons delineate a sustainable potential above 100%. These vast potentials are valuable assets for Vienna's urban energy development plans.

The circles on the maps in Fig. 6 indicate the different potentials of settlement development described in Vienna's new urban development plan called STEP 2025 [82]. The plan comprises 480 to 9400 new housing units in areas all over Vienna [81]. So far no (magenta circles) or only short branches (orange circles) of the DH system reach into these areas. Accordingly, shallow geothermal systems are revealed to be the ideal decentralised, renewable energy resource for these new housing units. The eastern and southern districts comprise the majority of the potential areas for settlement development. Moreover, here are also the areas with the highest BHE heat supply rate and sustainable potential. In regard to the smaller system spacing in the south-western city area, district 2, 10 and 11 are the most suitable areas for GWHP systems (Figure C.17). In the southern part of district 10, 5850 new housing units are planned in an area without a DH system and a high supply rates. The mere coincidence and winning combination of the three high potentials, namely geothermal, sustainable and settlement development potential, provide support for an easy assessment of feasibility and integration of geothermal system in local urban energy planning.

4. Conclusion

For this study, the Python and ArcGIS based tool GeoEnPy was developed and applied to the city of Vienna to compute the anthropogenic heat flux and flow into the urban subsurface, the technical geothermal potential for closed and open-loop systems, the sustainable potential, as well as the heat supply rate. Parameter uncertainties and spatial variability were assessed by performing Monte Carlo simulation. With GeoEnPy the most attractive locations for BHE and GWHP systems in Vienna with respect to existing heating infrastructure were identified. GeoEnPy relies on basic hydrogeological and city data, such as building stock and subsurface infrastructure information, and can therefore also be applied to other cities. To extend the geospatial analysis of GeoEnPy to a spatio-temporal analysis, seasonal and annual variations in heat and also cooling demands, as well as heat flow could be integrated in future studies. Furthermore, the theoretical sustainable and technical geothermal potential could be combined to investigate how much of the annual heat input could be technically extracted by BHE or GWHP.

The suburban districts 10, 12, 22 and 23 achieve high heat supply rates and the highest sustainable potential. Hence, these areas are the key locations for geothermal use in Vienna. In general, BHE systems achieve a higher supply rate than GWHP systems and are thus more attractive, due to the smaller spacing between the individual systems. The overall annual heat flow from anthropogenic heat sources in these four districts is 53% of the current heating demand. By extracting only this annually recharged thermal energy, a cooling of the ground and long-term reduction in system efficiency could be avoided. A further increase in efficiency and sustainability could be achieved by storing thermal energy in the subsurface, e.g. through borehole thermal energy storage (BTES) or aquifer thermal energy storage (ATES) systems and/or a combination with solar collectors. The illustration of the high geothermal and sustainable potentials, especially in case of closed-loop systems at the urban fringe, should encourage and support urban planners, energy agencies and public authorities to incorporate shallow geothermal energy in future urban development.

Data availability

Data sets related to this article can be found at https://digitales.wien.gv.at/site/open-data/ and are also listed in Table D.5 in the supplementary information of this article.

Author's contribution

CT acquired and analysed the data as well as wrote the manuscript. SB, KM, PBl and PBa provided scientific supervision and guidance for the research. Valuable revisions of the manuscript were made by SB, KM, PBl, PBa, CS and GG. CS also acquired data and established contact to local authorities for data interchange. All authors read and approved the final manuscript.

Declaration of competing interest

The authors declare that they have no known competing

financial interests or personal relationships that could have appeared to influence the work reported in this paper.

Acknowledgments

The authors are grateful for data exchange with Wiener Linien, Wien Energie, Technische Universität Wien and ZAMG (Zentralanstalt für Meteorologie und Geodynamik). The authors particularly thank Bernd Kowaschitz and Thilo Lehmann from Wien Kanal as well as Robert Lauter from Wien Energie for their informative conversations regarding sewage water temperature and heat loss rates of the local district heating network. We gratefully acknowledge the provision of tunnel data by Julia Della Porta from ASFINAG (Autobahnen-und Schnellstraßen-Finanzierungs-Aktiengesellschaft). The authors thank GRACE, the Graduate School for PhD students of the KIT-Centre Climate and Environment at the Karlsruhe Institute of Technology (KIT) and Helmholtz Association of German Research Centres (HGF) portfolio project "Geoenergy" (grant number 35.14.01; POF III, LK 01) for funding this work. We also thank the two reviewers for their comments.

Abbreviation

AHF	anthropogenic heat flux
BHE	borehole heat exchangers
DEM	digital elevation model
DH	district heating
GBA	Geological Survey of Austria
GIS	geographic information system
GSHP	ground source heat pump
GW	groundwater
GWHP	groundwater heat pump
GWT	groundwater temperature
GST	ground surface temperature
HD	heating demand
LU	land use
SUHI	subsurface urban heat island

Appendix A. Figures

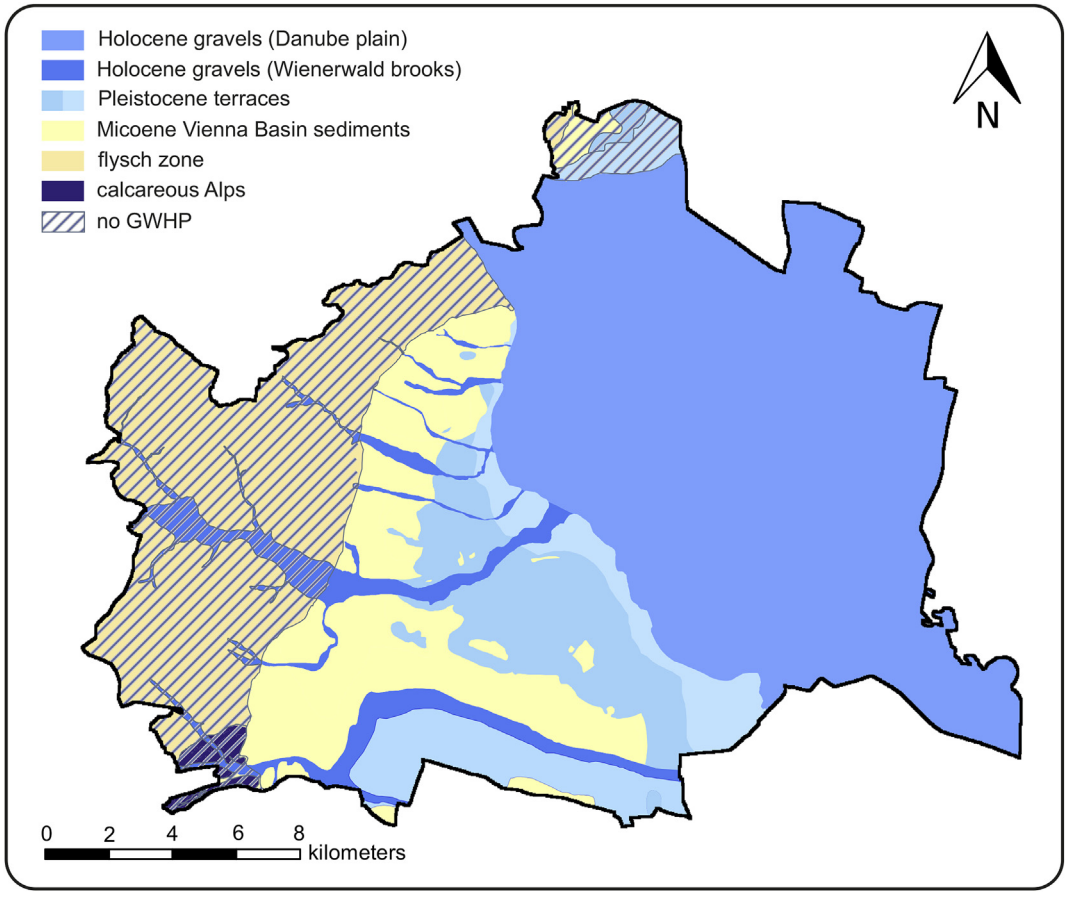

Figure A.7
Hydrogeological zones of Vienna (adapted from Götzl et al. [69]). The striped zone indicates the area without groundwater heat pump (GWHP) installations in this study.

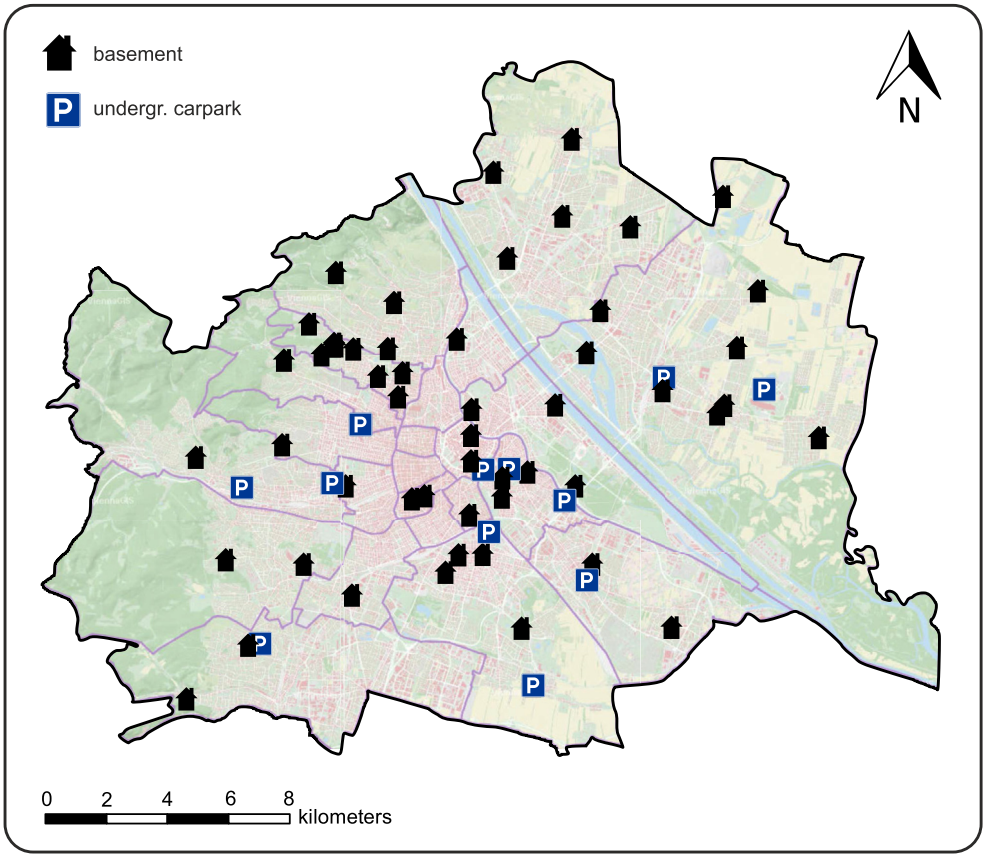

Figure A.8
Location of iButtons to measure the air temperature in basements and underground carparks.

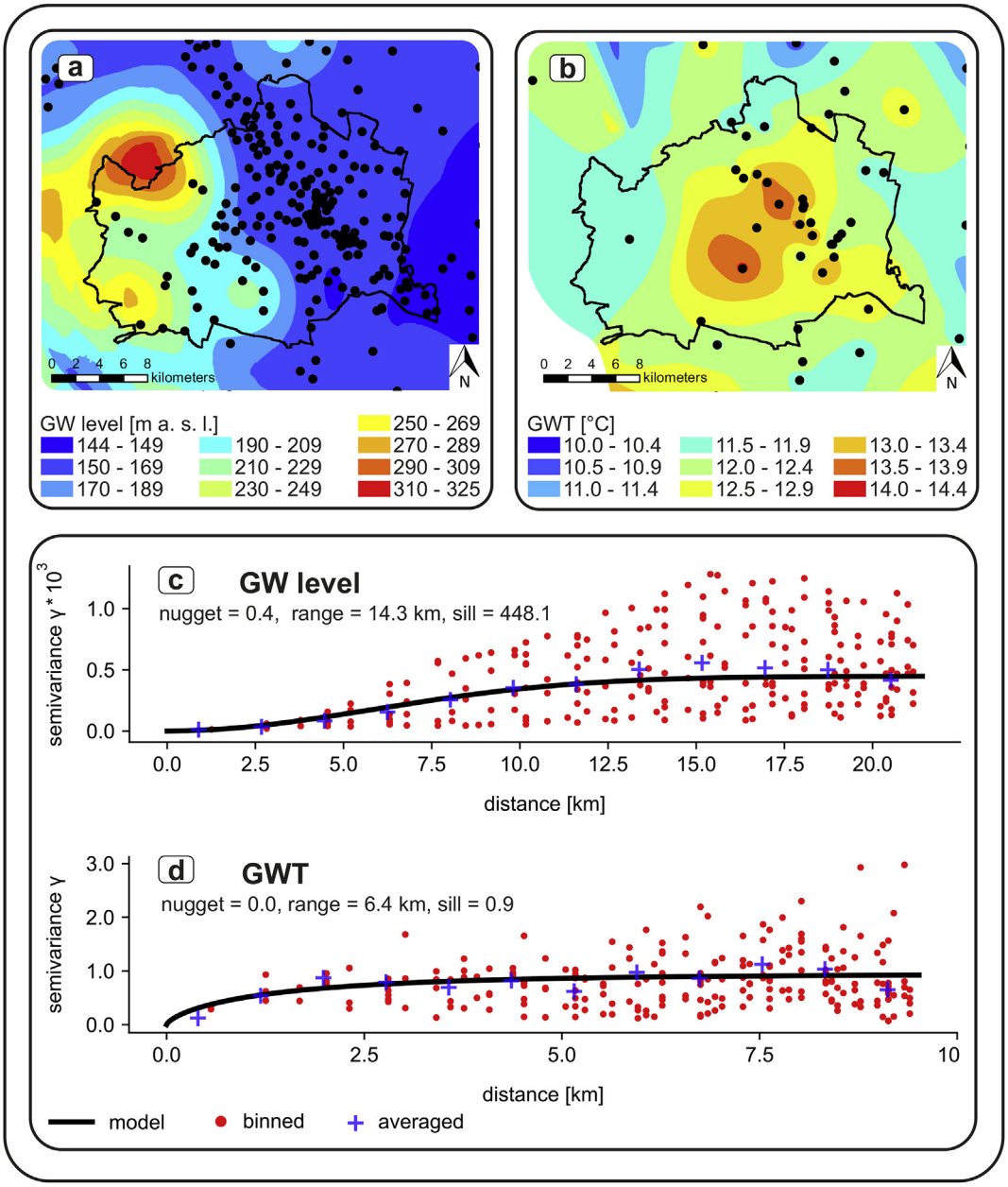

Figure A.9
Interpolated mean groundwater (GW) level (a) and groundwater temperature (GWT) (b) data from 2007 to 2016. Black points represent the measurement sites. Mean GW levels and GWT are 163.3 ± 19.1 m and 12.2 ± 1.0 °C. Maximum GW level (262.0 m) was measured in the north-western part of Vienna and the lowest (144.2 m) at the Danube River to the west of Vienna. The site with the highest GWT (14.5 °C) is south of the Central station, the site with the lowest GWT (10.2 °C) is in a forest north of Vienna. Ordinary kriging incorporating secondary data such as a digital elevation model (DEM) yielded the most accurate results of all tested geostatistical methods by Ohmer et al. [83]. Accordingly, in this study ordinary kriging including DEM was applied to interpolate GW level and GWT data. The interpolation of GWT and GW level data may lead to a weak prediction in areas with a low data density, i.e. a large distance between two measurement sites. A low density of measurement sites occurs in the western city parts, in particular for the GWT. The semivariograms (c, d) indicate that for distances larger than 14 km and 6 km for GW level and GWT measurements sites, respectively, correlation of the data is less significant.

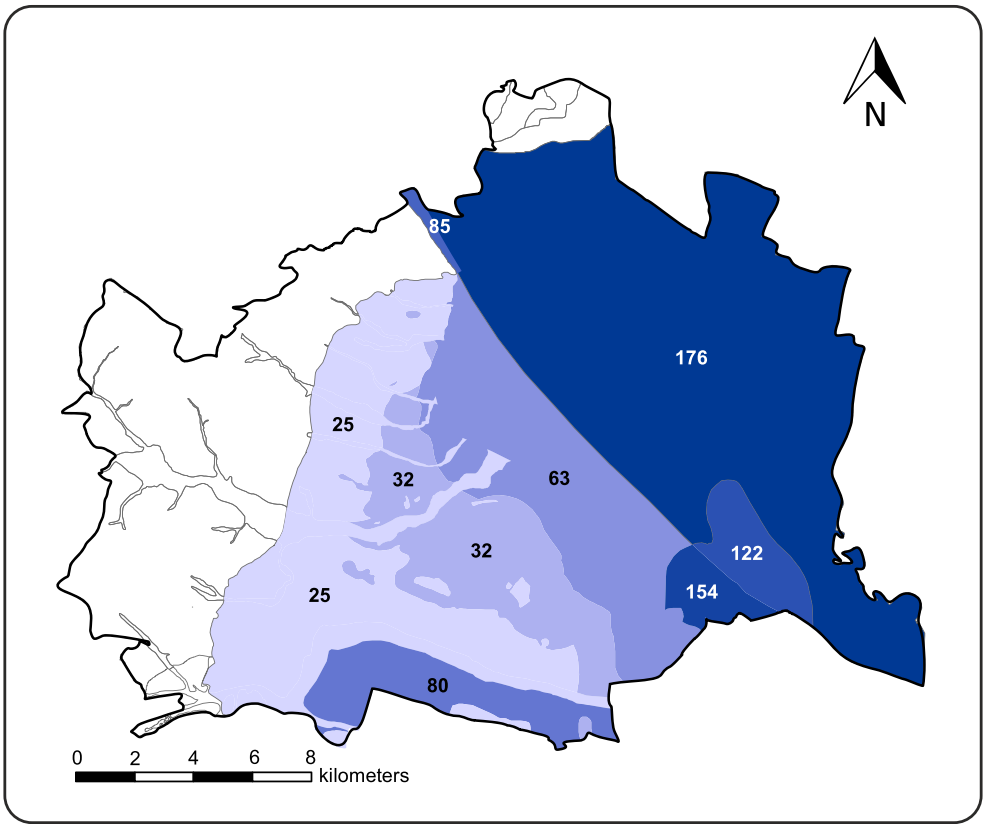

Figure A.10
The numbers indicate the maximum plume length of the ΔT = 1 K isotherm which defines the distance between groundwater heat pump systems. The estimation of the temperature plume extension of the cooled, reinjected water bases on the analytical approach by Kinzelbach [84].

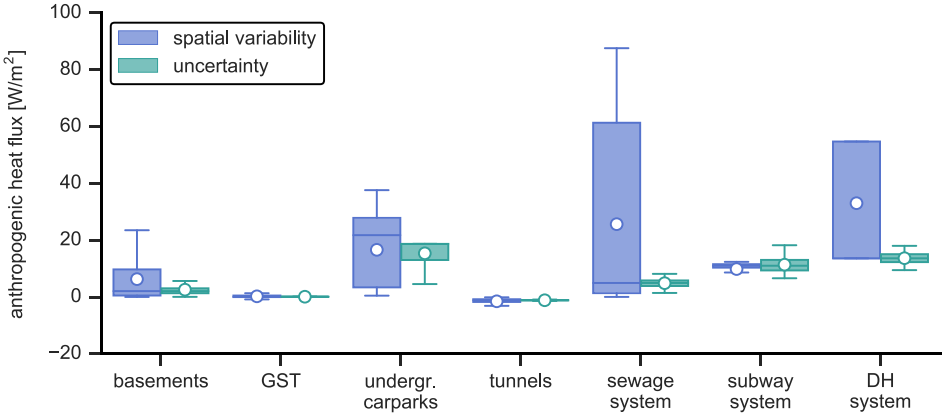

Figure A.11
Boxplots of the spatial variability and uncertainty of the individual anthropogenic heat fluxes. Mean values are indicated with a white dot. Abbreviations: ground surface temperature (GST), district heating system (DH).

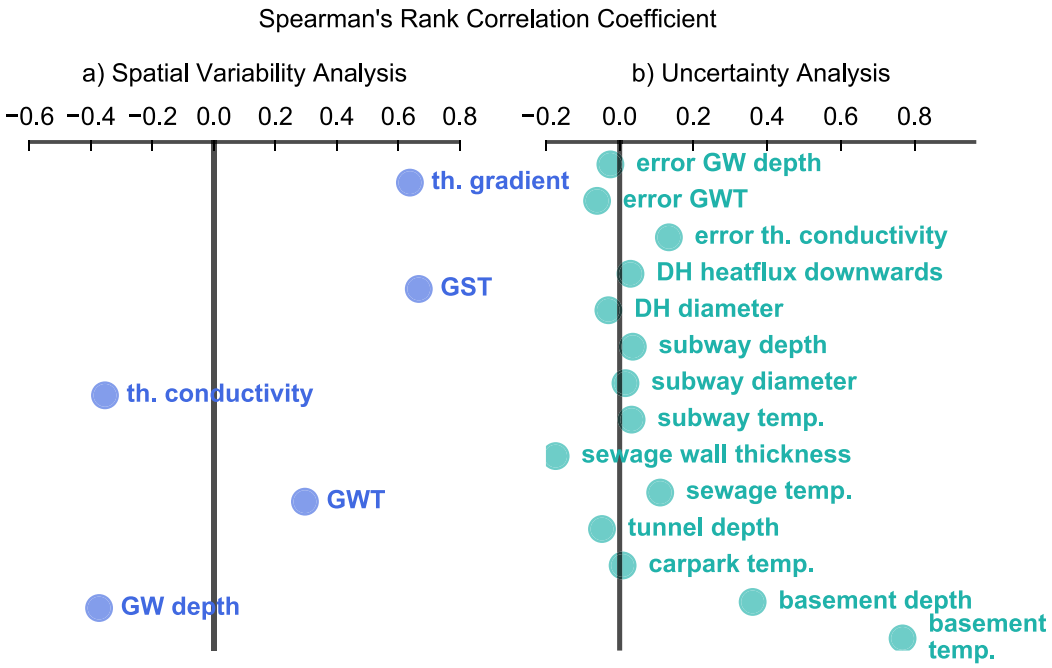

Figure A.12
Results of the spatial variability and uncertainty analysis. Spearman's rank correlation coefficients between the heat flux per pixel and the individual parameters (spatial variability) and between the heat flow and the individual parameters (parameter uncertainty). Abbreviations: groundwater (GW), groundwater temperature (GWT), ground surface temperature (GST), thermal (th.).

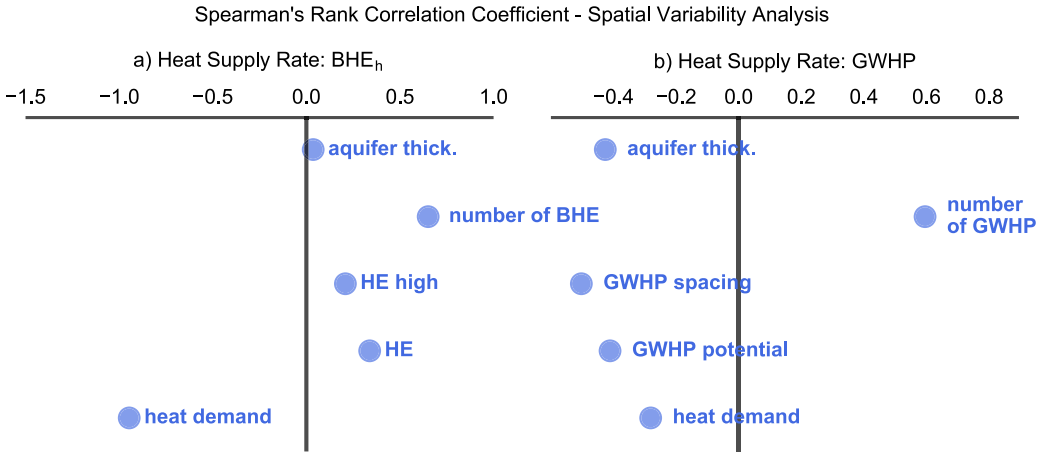

Figure A.13
Results of the spatial variability for borehole heat exchangers (BHEh) with higher heat extraction (HE) rate and groundwater heat pump (GWHP) systems. Spearman's rank correlation coefficients between the heat supply rate per hexagon and the individual parameters.

Appendix B. Tables

Table B.1
Input files and parameters with their values, units and sources applied in the Monte Carlo simulation, heat flux and heat supply rate calculation. Abbreviation: borehole heat exchangers (BHE), district heating (DH), ground surface temperature (GST), groundwater (GW), groundwater heat pump (GWHP), groundwater temperature (GWT), heating demand (HD).

input files and parameters	value	unit	reference
flux evaluation: ground surface temperature (GST)			
area of Vienna	shapefile		Stadt Wien
thermal conductivity 0–30 m	raster	W/mK	GBA[1]
thermal conductivity error	−0.20, 0.00, 0.20	W/mK	Götzl et al. [69]
digital elevation model	raster	m	Stadt Wien
air temperature	WFS	°C	ZAMG revised by GBA, GeoPLASMA-CE[1]
land use	shapefile		GMES
GWT	well data	°C	eHYD
error of GWT measurement	−0.10, 0.00, 0.10	°C	Benz et al. [46]
mean groundwater level	well data	m	eHYD
error of GW level measurement	−0.01, 0.00, 0.01	m	Benz et al. [46]
surface water	shapefile		Stadt Wien
bridges	shapefile		Stadt Wien
flux evaluation: building			
building footprints	shapefile		Stadt Wien
basement temperature	12.90, 15.70, 20.60	°C	iButton measurement
basement depth below ground	0.00, 2.50, 6.00	m	Benz et al. [46]
building: thickness of the floor	0.30	m	Benz et al. [46]
distance building – BHE	2.00	m	VDI 4640 part 2 [72]
flux evaluation: underground carpark			
undergr. carpark footprint	shapefile		derived from building footprint file
undergr. carpark temperatureture	12.90, 17.50, 21.80	°C	iButton measurement
undergr. carpark depth	shapfile	m	iButton measurement
undergr. carpark wall thickness	0.30	m	Benz et al. [46]
distance carpark – BHE	2.00	m	VDI 4640 part 2 [72]
flux evaluation: tunnel			
tunnel footprint	shapefile		Stadt Wien
tunnel temperature	WFS	°C	see air temperature
tunnel tube depth below ground	1.00, 1.50, 2.00	m	asfinag [85]
tunnel diameter	5.53	m	asfinag [85]
tunnel wall thickness	0.80	m	asfinag [85]
distance tunnel – BHE	2.00	m	VDI 4640 part 2 [72]
flux evaluation: sewage system			
sewage network	shapefile		Wien Kanal
sewage water temperature	14.20, 18.50, 21.50	°C	Wien Kanal
sewage pipe depth below ground	shapefile	m	Wien Kanal
sewage pipe diameter	shapefile	m	Wien Kanal
pipe wall thickness	0.02, 0.10, 0.32	m	Benz et al. [46], Wien Kanal
distance sewer - BHE	1.00	m	VDI 4640 part 2 [72]
flux evaluation: subway system			
subway network	shapefile		Stadt Wien
subway temperature	17.30, 19.00, 24.30	°C	Wiener Linien revised by GBA[1]
subway tube depth below ground	10.00, 20.00, 30.00	m	Wiener Linien [86]
subway tube diameter	6.90, 7.00, 7.30	m	Benz et al. [46]
subway tube wall thickness	1.10	m	Benz et al. [46]
distance subway – BHE	1.00	m	VDI 4640 part 2 [72]
flux evaluation: district heating (DH) system			
DH network	WFS		Wien Energie revised by GBA [1]
pipe diameter	0.17, 0.58, 1.00	m	Schmidt [87]
heat loss primary network	84.51	W/m	Wien Energie[2]
heat loss secondary network	21.04	W/m	Wien Energie[2]
heat flux directed downwards	25.00, 37.50, 50.00	%	Benz et al. [46]
pipe length	WFS	m	Wien Energie revised by GBA[1]
distance pipe - BHE	1.00	m	VDI 4640 part 2 [72]
evaluation of the heat supply rate			
HD un-/refurbished buildings	WFS	MWh/a	TU Wien revised by GBA[1]
coefficient of performance	4.00		Tissen et al. [49]
operation time	1800.00	h	VDI 4640 part 2 [72]
heat extraction rate (HE)	shapefile	W/m	Stadt Wien, SIA 384/6 [70]
HE high	shapefile	W/m	Stadt Wien, Erol [88]
HE error	shapefile	W/m	Stadt Wien,
HE high error	−5.00, 0.00, 5.00	W/m	deduced from therm. conduc. error
BHE length	150.00	m	GBA[1]
BHE spacing	10.00	m	GBA[1]
GWHP potential	shapefile	kW	Stadt Wien
GWHP spacing	shapefile	m	based on: Baden-Württemberg [89], Kinzelbach [84]
evaluation of the GWHP spacing			
retardation	2.00		Tissen et al. [49]
vol. heat capacity	2300000.00	$J/m^3/K$	GBA[1]
temperature reduction	5.00	K	Götzl et al. [69]
aquifer thickness	shapefile	m	GBA[1]

(*continued on next page*)

Table B.1 (*continued*)

input files and parameters	value	unit	reference
aquifer porosity	20.00	%	GBA[1]
hydraulic conductivity	shapefile	m/s	Umweltbundesamt GmbH [90]
Darcy velocity	raster	m/s	Darcy Velocity Tool[3]
groundwater flow velocity	shapefile	m/s	based on: Baden-Württemberg [89]
pumping rate	shapefile	m^3/s	based on: Baden-Württemberg [89]
longitudinal thermal dispersivity	shapefile	m	based on: Baden-Württemberg [89]
transversal thermal dispersivity	shapefile	m	based on: Baden-Württemberg [89]

[1] personal correspondence with Geological Survey of Austria (GBA).
[2] personal correspondence with Wien Energie.
[3] http://desktop.arcgis.com/en/arcmap/latest/tools/spatial-analyst-toolbox/darcy-velocity.htm.

Table B.2
Land use categories according to the Urban Atlas [68], their coverage rate and add on air temperature defined by Dědeček et al. [67] for the ground surface temperature estimation.

land use type	surface type			add on air temp. [°C]			coverage rate [%]
	sand and bare soil	grass	asphalt	min.	mode	max.	
continuous urban fabric (S.L. > 80%)	5	10	85	3.50	3.96	4.43	6.77
discontinuous dense urban fabric (S.L. 50%–80%)	10	25	65	2.80	3.23	3.65	9.07
discontinuous medium density (S.L. 30%–50%)	10	50	40	1.85	2.23	2.60	8.38
discontinuous low density urban (S.L. 10%–30%)	10	70	20	1.09	1.43	1.76	2.48
discontinuous very low density (S.L. < 10%)	10	85	5	0.52	0.83	1.13	0.10
isolated structures	0	0	100	4.00	4.50	5.00	0.10
industrial, commercial, public	5	0	95	3.88	4.36	4.85	12.54
fast transit roads and associated	0	0	100	4.00	4.50	5.00	0.51
other roads and associated land	0	0	100	4.00	4.50	5.00	6.20
railways and associated land	90	0	10	1.75	2.03	2.30	1.61
port areas	25	0	75	3.38	3.81	4.25	0.56
mineral extraction and dump sites	100	0	0	1.50	1.75	2.00	0.33
construction sites	100	0	0	1.50	1.75	2.00	0.55
land without current use	100	0	0	1.50	1.75	2.00	0.51
green urban areas	0	100	0	0.20	0.50	0.80	7.72
sports and leisure facilities	25	50	25	1.48	1.81	2.15	3.73
agricultural areas, semi-natural	50	50	0	0.85	1.13	1.40	17.01
forests	0	100	0	0.20	0.50	0.80	18.28
water	0	0	0	none			3.55

Table B.3
Spearman's rank correlation coefficient ρ and p-value for the spatial analysis and the uncertainty analysis of the heat flux. Abbreviation: district heating (DH), ground surface temperature (GST), groundwater (GW), groundwater temperature (GWT).

parameter	ρ	p-value
spatial variability		
GW depth	−0.37	0.00
GWT	0.29	0.00
th. conductivity	−0.35	0.00
GST	0.67	0.00
th. gradient	0.64	0.00
uncertainty		
basement temp.	0.77	0.00
basement depth	0.36	0.00
undergr. carpark temp.	0.01	0.80
tunnel depth	−0.05	0.13
sewage water temp.	0.11	0.00
sewer wall thickness	- 0.17	0.00
subway air temp.	0.03	0.31
subway tube diameter	0.02	0.62
subway depth	0.04	0.26
DH diameter	−0.03	0.33
DH flux downwards	0.03	0.35
error GW level	−0.03	0.43
error GWT	−0.06	0.05
error th. conductivity	0.13	0.00

Table B.4
Spearman's rank correlation coefficient ρ and p-value for the spatial analysis of the heat supply rate.

parameter	ρ	p-value
borehole heat exchanger BHE		
heating demand	−0.95	0.00
gross floor area	0.94	0.00
heat extraction	0.34	0.00
heat extraction high	0.21	0.00
nr. of BHE	0.65	0.00
aquifer thicknes	0.04	0.00
groundwater heat pump GWHP		
heating demand	−0.28	0.00
GWHP potential	−0.41	0.00
GWHP spacing	−0.50	0.00
nr. of GWHP	0.60	0.00
aquifer thickness	−0.43	0.00

References

[1] European Union (EU), Directive (EU) 2018/2001 of the European Parliament and of the Council - of 11 December 2018 - on the Promotion of the Use of Energy from Renewable Sources, 2018.
[2] Erneuerbare Energie Österreich, Positionspapier Wärmewende - ein Konzept des Dachverbandes Erneuerbare Energie Österreich, Tech. Rep, Wien, URL,

https://static1.squarespace.com/static/5b978be0697a98a663136c47/t/5c62a74ef4e1fcf05b96067a/1549969241083/Positionspapier+Wa%CC%88rmewende.pdf, 2019.
[3] Stadt wien, smart city wien, rahmenstrategie, tech. Rep., magistrat der Stadt wien, wien, URL, https://www.wien.gv.at/stadtentwicklung/studien/pdf/b008380a.pdf, 2016.
[4] Stadt Wien, Energy Framework Strategy 2030 for Vienna, Tech, Rep., Vienna, 2017. URL, https://www.wien.gv.at/stadtentwicklung/energie/pdf/energierahmenstrategie-2030-en.pdf.
[5] Stadt Wien, Smart City Wien Rahmenstrategie 2019-2050 - Die Wiener Strategie für eine nachhaltige Entwicklung, Tech. Rep., Wien, 2019.
[6] P. Blum, G. Campillo, W. Münch, T. Kölbel, CO2 savings of ground source heat pump systems – a regional analysis, ISSN 09601481, Renew. Energy 35 (1) (2010) 122–127, https://doi.org/10.1016/j.renene.2009.03.034. URL, http://linkinghub.elsevier.com/retrieve/pii/S0960148109003024.
[7] R. McMahon, H. Santos, Z.S. Mourão, Practical considerations in the deployment of ground source heat pumps in older properties—a case study, 03787788, Energy Build. 159 (2018) 54–65, https://doi.org/10.1016/j.enbuild.2017.08.067. URL, http://linkinghub.elsevier.com/retrieve/pii/S0378778817311106.
[8] J.W. Lund, T.L. Boyd, Direct utilization of geothermal energy 2015 worldwide review, ISSN 03756505, Geothermics 60 (2016) 66–93, https://doi.org/10.1016/j.geothermics.2015.11.004. URL, http://linkinghub.elsevier.com/retrieve/pii/S037565051500156X.
[9] P. Bayer, D. Saner, S. Bolay, L. Rybach, P. Blum, Greenhouse gas emission savings of ground source heat pump systems in Europe: a review, ISSN 13640321, Renew. Sustain. Energy Rev. 16 (2) (2012) 1256–1267, https://doi.org/10.1016/j.rser.2011.09.027. URL, http://linkinghub.elsevier.com/retrieve/pii/S1364032111004771.
[10] M. Jakob, K. Flury, N. Gross, G. Martius, B. Sunarjo, Kurzbericht Konzept Energieversorgung 2050: Szenarien für eine 2000-Watt-kompatible Wärmeversorgung für die Stadt Zürich, Tech. Rep, Departement der Industriellen Betriebe, Zürich, 2014. URL, https://nheeren.github.io/publication/jakob-2014-b/jakob-2014-b.pdf.
[11] H. Lund, B. Möller, B. Mathiesen, A. Dyrelund, The role of district heating in future renewable energy systems, ISSN 03605442, Energy 35 (3) (2010) 1381–1390, https://doi.org/10.1016/j.energy.2009.11.023. URL, https://linkinghub.elsevier.com/retrieve/pii/S036054420900512X.
[12] G.B.A. GBA, Geologische bundesanstalt, URL, https://www.geologie.ac.at/ueber-uns/unser-haus/standort/.
[13] F. Stauffer, P. Bayer, P. Blum, N. Molina-Giraldo, W. Kinezlbach, Thermal Use of Shallow Groundwater, CRC Press, S.l., 2014, ISBN 978-1-138-07785-0 oCLC: 1020635550.
[14] F. Böttcher, A. Casasso, G. Götzl, K. Zosseder, TAP - thermal aquifer Potential: a quantitative method to assess the spatial potential for the thermal use of groundwater, ISSN 09601481, Renew. Energy 142 (2019) 85–95, https://doi.org/10.1016/j.renene.2019.04.086. URL, https://linkinghub.elsevier.com/retrieve/pii/S0960148119305701.
[15] J. Luo, Z. Luo, J. Xie, D. Xia, W. Huang, H. Shao, W. Xiang, J. Rohn, Investigation of shallow geothermal potentials for different types of ground source heat pump systems (GSHP) of Wuhan city in China, URL, Renew. Energy 118 (2018) 230–244, https://doi.org/10.1016/j.renene.2017.11.017. ISSN 09601481, http://linkinghub.elsevier.com/retrieve/pii/S0960148117311187.
[16] A. Sbrana, P. Marianelli, G. Pasquini, P. Costantini, F. Palmieri, V. Ciani, M. Sbrana, The integration of 3D modeling and simulation to determine the energy potential of low-temperature geothermal systems in the Pisa (Italy) sedimentary plain, ISSN 1996-1073, Energies 11 (6) (2018) 1591, https://doi.org/10.3390/en11061591. URL, http://www.mdpi.com/1996-1073/11/6/1591.
[17] Y. Noorollahi, H. Gholami Arjenaki, R. Ghasempour, Thermo-economic modeling and GIS-based spatial data analysis of ground source heat pump systems for regional shallow geothermal mapping, ISSN 13640321, Renew. Sustain. Energy Rev. 72 (2017) 648–660, https://doi.org/10.1016/j.rser.2017.01.099. URL, http://linkinghub.elsevier.com/retrieve/pii/S1364032117301077.
[18] A. Casasso, R. Sethi, G. POT, A quantitative method for the assessment and mapping of the shallow geothermal potential, ISSN 0360-5442, Energy 106 (Supplement C) (2016) 765–773, https://doi.org/10.1016/j.energy.2016.03.091. URL, http://www.sciencedirect.com/science/article/pii/S0360544216303358.
[19] P. Bayer, G. Attard, P. Blum, K. Menberg, The geothermal potential of cities, ISSN 13640321, Renew. Sustain. Energy Rev. 106 (17–30) (2019), https://doi.org/10.1016/j.rser.2019.02.019. URL, https://linkinghub.elsevier.com/retrieve/pii/S1364032119301121.
[20] A. Gemelli, A. Mancini, S. Longhi, GIS-based energy-economic model of low temperature geothermal resources: a case study in the Italian Marche region, ISSN 0960-1481, Renew. Energy 36 (9) (2011) 2474–2483, https://doi.org/10.1016/j.renene.2011.02.014. URL, http://www.sciencedirect.com/science/article/pii/S0960148111000905.
[21] A. García-Gil, E. Vázquez-Suñe, M.M. Alcaraz, A.S. Juan, J.n. Sánchez-Navarro, M. Montlleó, G. Rodríguez, J. Lao, GIS-supported mapping of low-temperature geothermal potential taking groundwater flow into account, ISSN 0960-1481, Renew. Energy 77 (Supplement C) (2015) 268–278, https://doi.org/10.1016/j.renene.2014.11.096. URL, http://www.sciencedirect.com/science/article/pii/S0960148114008477.
[22] J. Ondreka, M.I. Rüsgen, I. Stober, K. Czurda, GIS-supported mapping of shallow geothermal potential of representative areas in south-western Germany—Possibilities and limitations, ISSN 09601481, Renew. Energy 32 (13) (2007) 2186–2200, https://doi.org/10.1016/j.renene.2006.11.009. URL, http://linkinghub.elsevier.com/retrieve/pii/S0960148106003338.
[23] B. Meng, T. Vienken, O. Kolditz, H. Shao, Evaluating the thermal impacts and sustainability of intensive shallow geothermal utilization on a neighborhood scale: lessons learned from a case study, ISSN 01968904, Energy Convers. Manag. 199 (2019), 111913, https://doi.org/10.1016/j.enconman.2019.111913. URL, https://linkinghub.elsevier.com/retrieve/pii/S0196890419309045.
[24] T. Vienken, S. Schelenz, K. Rink, P. Dietrich, Sustainable intensive thermal use of the shallow subsurface-A critical view on the status quo, ISSN 0017467X, Groundwater 53 (3) (2015) 356–361, https://doi.org/10.1111/gwat.12206. URL.
[25] T. Kurevija, D. Vulin, V. Krapec, Effect of borehole array geometry and thermal interferences on geothermal heat pump system, ISSN 0196-8904, Energy Convers. Manag. 60 (2012) 134–142, https://doi.org/10.1016/j.enconman.2012.02.012. URL, http://www.sciencedirect.com/science/article/pii/S0196890412000702.
[26] C. Zhang, Y. Wang, Y. Liu, X. Kong, Q. Wang, Computational methods for ground thermal response of multiple borehole heat exchangers: a review, ISSN 0960-1481, Renew. Energy 127 (2018) 461–473, https://doi.org/10.1016/j.renene.2018.04.083. URL, http://www.sciencedirect.com/science/article/pii/S0960148118305081.
[27] A.M. Patton, G. Farr, D.P. Boon, D.R. James, B. Williams, L. James, R. Kendall, S. Thorpe, G. Harcombe, D.I. Schofield, A. Holden, D. White, Establishing an urban geo-observatory to support sustainable development of shallow subsurface heat recovery and storage, 49–61, ISSN 1470-9236, Q. J. Eng. Geol. Hydrogeol. 53 (1) (2020) 2041–4803, https://doi.org/10.1144/qjegh2019-020. URL, http://qjegh.lyellcollection.org/lookup/doi/10.1144/qjegh2019-020.
[28] G. Ferguson, A.D. Woodbury, Observed thermal pollution and post-development simulations of low-temperature geothermal systems in Winnipeg, Canada, 1206–1215, ISSN 1431-2174, 1435-0157, Hydrogeol. J. 14 (7) (2006), https://doi.org/10.1007/s10040-006-0047-y. URL, http://link.springer.com/10.1007/s10040-006-0047-y.
[29] H.C. Bonsor, P. Dahlqvist, L. Moosmann, N. Classen, J. Epting, P. Huggenberger, A. Garica-Gil, M. Janźa, G. Laursen, R. Stuurman, C.R. Gogu, Geothermal modelling and monitoring at city-scales – identifying good practice, and effective knowledge exchange, Tech. Rep., Britsh Geological Survey Open Report (2017) 69.
[30] M. Abu-Rumman, M. Hamdan, O. Ayadi, Performance enhancement of a photovoltaic thermal (PVT) and ground-source heat pump system, Geothermics 85 (2020), 101809, https://doi.org/10.1016/j.geothermics.2020.101809. ISSN 03756505, https://linkinghub.elsevier.com/retrieve/pii/S0375650518303626.
[31] A. Georgiev, R. Popov, E. Toshkov, Investigation of a hybrid system with ground source heat pump and solar collectors: charging of thermal storages and space heating, ISSN 09601481, Renew. Energy 147 (2020) 2774–2790, https://doi.org/10.1016/j.renene.2018.12.087. URL, https://linkinghub.elsevier.com/retrieve/pii/S0960148118315337.
[32] S.A. Benz, P. Bayer, P. Blum, H. Hamamoto, H. Arimoto, M. Taniguchi, Comparing anthropogenic heat input and heat accumulation in the subsurface of Osaka, Japan, ISSN 00489697, Sci. Total Environ. 643 (2018) 1127–1136, https://doi.org/10.1016/j.scitotenv.2018.06.253. URL, https://linkinghub.elsevier.com/retrieve/pii/S0048969718323295.
[33] M.H. Mueller, P. Huggenberger, J. Epting, Combining monitoring and modelling tools as a basis for city-scale concepts for a sustainable thermal management of urban groundwater resources, ISSN 00489697, Sci. Total Environ. 627 (2018) 1121–1136, https://doi.org/10.1016/j.scitotenv.2018.01.250. URL, http://linkinghub.elsevier.com/retrieve/pii/S0048969718302924.
[34] J. Epting, F. Böttcher, M.H. Mueller, A. García-Gil, K. Zosseder, P. Huggenberger, City-scale solutions for the energy use of shallow urban subsurface resources – bridging the gap between theoretical and technical potentials, ISSN 09601481, Renew. Energy 147 (2020) 751–763, https://doi.org/10.1016/j.renene.2019.09.021. URL, https://linkinghub.elsevier.com/retrieve/pii/S0960148119313515.
[35] J.A. Rivera, P. Blum, P. Bayer, Analytical simulation of groundwater flow and land surface effects on thermal plumes of borehole heat exchangers, ISSN 03062619, Appl. Energy 146 (2015) 421–433, https://doi.org/10.1016/j.apenergy.2015.02.035. URL, http://linkinghub.elsevier.com/retrieve/pii/S0306261915002123.
[36] K. Balke, Das grundwasser als energieträger, Brennst. Wärme Kraft 29 (1977) 191–194.
[37] G. Ferguson, A.D. Woodbury, Subsurface heat flow in an urban environment, ISSN 2156-2202, J. Geophys. Res.: Solid Earth 109 (B2) (2004) B02402, https://doi.org/10.1029/2003JB002715. URL, http://onlinelibrary.wiley.com/doi/10.1029/2003JB002715/abstract.
[38] J. Epting, S. Scheidler, A. Affolter, P. Borer, M.H. Mueller, L. Egli, A. García-Gil, P. Huggenberger, The thermal impact of subsurface building structures on urban groundwater resources – a paradigmatic example, ISSN 00489697, Sci. Total Environ. 596–597 (2017) 87–96, https://doi.org/10.1016/j.scitotenv.2017.03.296. URL, http://linkinghub.elsevier.com/retrieve/pii/S0048969717308276.
[39] D. Krcmar, R. Flakova, I. Ondrejkova, K. Hodasova, D. Rusnakova, Z. Zenisova,

M. Zatlakovic, Assessing the Impact of a Heated Basement on Groundwater Temperatures in Bratislava, gwat.12986ISSN 0017-467X, Groundwater, Slovakia, 2020, pp. 1745–6584, https://doi.org/10.1111/gwat.12986. URL, https://onlinelibrary.wiley.com/doi/abs/10.1111/gwat.12986.
[40] A. Bidarmaghz, R. Choudhary, K. Soga, H. Kessler, R.L. Terrington, S. Thorpe, Influence of geology and hydrogeology on heat rejection from residential basements in urban areas, ISSN 08867798, Tunn. Undergr. Space Technol. 92 (2019) 103068, https://doi.org/10.1016/j.tust.2019.103068. URL, https://linkinghub.elsevier.com/retrieve/pii/S0886779818309635.
[41] H. Hemmerle, S. Hale, I. Dressel, S.A. Benz, G. Attard, P. Blum, P. Bayer, Estimation of groundwater temperatures in Paris, France, ISSN 1468-8115, Geofluids 1–11 (2019) 1468–8123, https://doi.org/10.1155/2019/5246307, 2019, URL, https://www.hindawi.com/journals/geofluids/2019/5246307/.
[42] G. Ferguson, A.D. Woodbury, Urban heat island in the subsurface, ISSN 1944-8007, Geophys. Res. Lett. 34 (23) (2007) L23713, https://doi.org/10.1029/2007GL032324. URL, http://onlinelibrary.wiley.com/doi/10.1029/2007GL032324/abstract.
[43] M. Taniguchi, J. Shimada, Y. Fukuda, M. Yamano, S.-i. Onodera, S. Kaneko, A. Yoshikoshi, Anthropogenic effects on the subsurface thermal and groundwater environments in Osaka, Japan and Bangkok, Thailand, ISSN 00489697, Sci. Total Environ. 407 (9) (2009) 3153–3164, https://doi.org/10.1016/j.scitotenv.2008.06.064. URL, http://linkinghub.elsevier.com/retrieve/pii/S0048969708006852.
[44] C.A. Taylor, H.G. Stefan, Shallow groundwater temperature response to climate change and urbanization, ISSN 00221694, J. Hydrol. 375 (3–4) (2009) 601–612, https://doi.org/10.1016/j.jhydrol.2009.07.009. URL, http://linkinghub.elsevier.com/retrieve/pii/S0022169409004004.
[45] K. Menberg, P. Bayer, K. Zosseder, S. Rumohr, P. Blum, Subsurface urban heat islands in German cities, ISSN 00489697, Sci. Total Environ. 442 (2013a) 123–133, https://doi.org/10.1016/j.scitotenv.2012.10.043. URL, http://linkinghub.elsevier.com/retrieve/pii/S0048969712013253.
[46] S.A. Benz, P. Bayer, K. Menberg, S. Jung, P. Blum, Spatial resolution of anthropogenic heat fluxes into urban aquifers, ISSN 0048-9697, Sci. Total Environ. 524–525 (2015) 427–439, https://doi.org/10.1016/j.scitotenv.2015.04.003. URL, http://www.sciencedirect.com/science/article/pii/S0048969715004398.
[47] J.A. Rivera, P. Blum, P. Bayer, Increased ground temperatures in urban areas: estimation of the technical geothermal potential, ISSN 09601481, Renew. Energy 103 (2017) 388–400, https://doi.org/10.1016/j.renene.2016.11.005. URL, http://linkinghub.elsevier.com/retrieve/pii/S0960148116309673.
[48] K. Zhu, P. Blum, G. Ferguson, K.-D. Balke, P. Bayer, The geothermal potential of urban heat islands, Environ. Res. Lett., 5, ISSN 1748-9326, doi:10.1088/1748-9326/6/1/019501, URL, http://stacks.iop.org/1748-9326/6/i=1/a=019501?key=crossref.19fcdd27f8d3632148f6e29f16a148a0.
[49] C. Tissen, K. Menberg, P. Bayer, P. Blum, Meeting the demand: geothermal heat supply rates for an urban quarter in Germany, Geoth. Energy, 7 (1), ISSN 2195-9706, doi:10.1186/s40517-019-0125-8, URL, https://geothermal-energy-journal.springeropen.com/articles/10.1186/s40517-019-0125-8.
[50] Y. Zhang, K. Soga, R. Choudhary, Shallow geothermal energy application with GSHPs at city scale: study on the City of Westminster, ISSN 2045-2543, Géotech. Lett. 4 (2) (2014) 125–131, https://doi.org/10.1680/geolett.13.00061. URL, http://www.icevirtuallibrary.com/doi/10.1680/geolett.13.00061.
[51] S. Miglani, K. Orehounig, J. Carmeliet, A methodology to calculate long-term shallow geothermal energy potential for an urban neighbourhood, ISSN 03787788, Energy Build. 159 (2018) 462–473, https://doi.org/10.1016/j.enbuild.2017.10.100. URL, http://linkinghub.elsevier.com/retrieve/pii/S0378778817317450.
[52] K. Schiel, O. Baume, G. Caruso, U. Leopold, GIS-based modelling of shallow geothermal energy potential for CO 2 emission mitigation in urban areas, ISSN 09601481, Renew. Energy 86 (2016) 1023–1036, https://doi.org/10.1016/j.renene.2015.09.017. URL, http://linkinghub.elsevier.com/retrieve/pii/S0960148115302962.
[53] H. Kupfersberger, G. Rock, J.C. Draxler, Inferring near surface soil temperature time series from different land uses to quantify the variation of heat fluxes into a shallow aquifer in Austria, ISSN 00221694, J. Hydrol. 552 (2017) 564–577, https://doi.org/10.1016/j.jhydrol.2017.07.030. URL, http://linkinghub.elsevier.com/retrieve/pii/S002216941730481X.
[54] S. Pfleiderer, T. Hofmann, Digitaler angewandter Geo-Atlas der Stadt Wien - Projekt WC 21 HYDRO-Modul, Tech. Rep., Geological Survey of Austria, Wien, 2004.
[55] S. Pfleiderer, Hydrochemistry of Groundwater in the City of Vienna, 2019. Austria.
[56] S. Pfleiderer, T. Hofmann, Digitaler angewandter geo-atlas – stadtgeologie am beispiel von Wien, ISSN 0016–7800, Jb. Geol. B.-A. 147 (Heft 1+2) (2007) 263–273.
[57] Stadt Wien, data.gv.at - offene Daten Österreichs – lesbar für Mensch und Maschine, URL, https://www.data.gv.at/.
[58] eHYD, eHYD – der Zugang zu hydrographischen Daten Österreichs, URL, https://ehyd.gv.at/.
[59] eHYD, Hydrographisches Jahrbuch Von Österreich 2015 – Erläuterungen UWQ, Tech. Rep., Bundesministerium für Nachhaltigkeit und Tourismus, Wien, 2015.
[60] Wiener Linien, Unternehmen | Wiener linien, URL, http://%3A%2F%2Fwww.wienerlinien.at%2Feportal3%2Fep%2Ftab.do%3FpageTypeId%3D66528a.
[61] Wien Kanal, KANIS - kanalinformationssystem, URL, http://www.kanis.at/.
[62] Wiener Stadtwerke, Nachhaltigkeitsbericht, Unsere Verantwortung für Generationen, Tech. Rep. (2017) 118. Wien, URL, https://www.wienerstadtwerke.at/eportal3/ep/programView.do/pageTypeId/71283/programId/3600227/channelId/-49476, 2018.
[63] MA 20, Energie! voraus - Energiebericht der Stadt Wien, 2019, p. 76.
[64] Österreichisches Institut für Bautechnik, OIB Richtlinie 6 Energieeinsparung und Wärmeschutz, 2015.
[65] S. Hartmann, Transform+ Transformationsplan Wien, Tech. Rep., Magistratsabteilung MA 18 - stadtentwicklung und Stadtplanung, Wien. https://www.transform-plus.at/fileadmin/user_upload/Dokumente2/D_1.3_Transformationsplan_10.pdf, 2016.
[66] ZAMG, SPARTACUS, URL, https://www.zamg.ac.at/cms/de/forschung/klima/klimatografien/spartacushttp://link.springer.com/10.1007/s00704-015-1411-4.
[67] P. Dědeček, J. Šafanda, D. Rajver, Detection and quantification of local anthropogenic and regional climatic transient signals in temperature logs from Czechia and Slovenia, ISSN 0165-0009, 1573-1480, Climatic Change 113 (3–4) (2012) 787–801, https://doi.org/10.1007/s10584-011-0373-5. URL, http://link.springer.com/10.1007/s10584-011-0373-5.
[68] GMES, Urban Atlas, URL, https://www.eea.europa.eu/data-and-maps/data/urban-atlas.
[69] G. Götzl, M. Fuchsluger, F.A. Rodler, P. Lipiarski, S. Pfleiderer, Projekt WC-31 Erdwärmepotenzialerhebung Stadtgebiet Wien, Modul 1 Endbericht, Tech. Rep., Magistrat der Stadt Wien Magistratsabteilung 20 – Energieplanung, 2014. Wien.
[70] SIA, Erdwärmesonden, 2009, 384/6.
[71] VDI 4640 part 2, Thermische Nutzung des Untergrundes - Erdgekoppelte Wärmepumpenanlagen, Beuth Verlag, Berlin, 2001. URL, http://perinorm-s.redi-bw.de/volltexte/CD22DE01/9197793/9197793.pdf?.
[72] VDI 4640 part 2, Thermische Nutzung des Untergrunds - Erdgekoppelte Wärmepumpenanlagen, Beuth Verlag, Berlin, 2015. URL, http://perinorm-fr.redi-bw.de/volltexte/CD22DE02/2313926/2313926.pdf?.
[73] Wiener Stadtwerke, Wie die Wiener Stadtwerke wirken, Tech. Rep., Wiener Stadtwerke, Wien, URL, https://www.wienerstadtwerke.at/media/files/2016/wstw%20nachhaltigkeitsbericht%202015_196261.pdf, 2015.
[74] J. Epting, F. Händel, P. Huggenberger, Thermal management of an unconsolidated shallow urban groundwater body, ISSN 1607-7938, Hydrol. Earth Syst. Sci. 17 (5) (2013) 1851–1869, https://doi.org/10.5194/hess-17-1851-2013. URL, http://www.hydrol-earth-syst-sci.net/17/1851/2013/.
[75] K.-H. Dahlem, The effect of groundwater on the heat loss of building parts in contact with the ground, Ph.D. thesis, Bauphysik/Technische Gebäudeausrüstung/Baulicher Brandschutz, Universität Kaiserslautern, 2000.
[76] K. Menberg, P. Blum, A. Schaffitel, P. Bayer, Long-term evolution of anthropogenic heat fluxes into a subsurface urban heat island, 9747–9755, ISSN 0013-936X, Environ. Sci. Technol. 47 (17) (2013b) 1520–5851, https://doi.org/10.1021/es401546u. URL, http://pubs.acs.org/doi/abs/10.1021/es401546u.
[77] M. Beck, P. Bayer, M. de Paly, J. Hecht-Méndez, A. Zell, Geometric arrangement and operation mode adjustment in low-enthalpy geothermal borehole fields for heating, URL, Energy 49 (2013) 434–443, https://doi.org/10.1016/j.energy.2012.10.060. ISSN 03605442, http://linkinghub.elsevier.com/retrieve/pii/S036054421200847X.
[78] W. Pophillat, G. Attard, P. Bayer, J. Hecht-Méndez, P. Blum, Analytical solutions for predicting thermal plumes of groundwater heat pump systems, Renewable Energy ISSN 09601481, doi:10.1016/j.renene.2018.07.148, URL, https://linkinghub.elsevier.com/retrieve/pii/S0960148118309455.
[79] I. Dochev, I. Peters, Potential for utilising near surface geothermal heat via heat pumps. A case study from Hamburg, Kassel 10 (2019).
[80] J. Epting, M.H. Müller, D. Genske, P. Huggenberger, Relating groundwater heat-potential to city-scale heat-demand: a theoretical consideration for urban groundwater resource management, ISSN 03062619, Appl. Energy 228 (2018) 1499–1505, https://doi.org/10.1016/j.apenergy.2018.06.154. URL, https://linkinghub.elsevier.com/retrieve/pii/S0306261918310134.
[81] E. Kail, Smart City Wien – Stadtentwicklungsplan 2025, 2017. URL, https://www.axel-troost.de/kontext/controllers/document.php/3356.0/5/086d67.pdf.
[82] MA 18, Step 2025 - stadtentwicklungsplan Wien, Tech. Rep., Magistratsabteilung MA 18 - stadtentwicklung und Stadtplanung, Wien, URL, https://www.wien.gv.at/stadtentwicklung/studien/pdf/b008379a.pdf, 2014.
[83] M. Ohmer, T. Liesch, N. Goeppert, N. Goldscheider, On the optimal selection of interpolation methods for groundwater contouring: an example of propagation of uncertainty regarding inter-aquifer exchange, Adv. Water Resour. 109 (2017) 121–132.
[84] W. Kinzelbach, Numerische Methoden zur Modellierung des Transports von Schadstoffen im Grundwasser, Oldenbourg Verlag, München, 1992.
[85] asfinag, Autobahnen- und Schnellstraßen-Finanzierungs-Aktiengesellschaft, URL, https://www.asfinag.at/.

[86] Wiener Linien, So tief fährt die U-Bahn, URL, https://www.wienerlinien.at/media/files/2016/u2u5_tiefe_neubaugasse_179582.pdfb.
[87] R.-R. Schmidt, Thermische netzwerke/fernwärme, URL, http://pubdb.ait.ac.at/files/PubDat_AIT_131314.pdf, 2011.
[88] S. Erol, Estimation of Heat Extraction Rates of GSHP Systems under Different Hydrogelogical Conditions, Masterarbeit, Universität Tübingen, Tübingen, 2011.
[89] Baden-Württemberg, Arbeitshilfe zum Leitfaden zur Nutzung von Erdwärme mit Grundwasserwärmepumpen. Tech. Rep., Umweltministerium Baden-Württemberg, Stuttgart, 2009. URL, https://um.baden-wuerttemberg.de/fileadmin/redaktion/m-um/intern/Dateien/Dokumente/5_Energie/Erneuerbare_Energien/Geothermie/4_Arbeitshilfe_zum_Leitfaden.pdf.
[90] Umweltbundesamt GmbH, H2O fachdatenbank - grundwasserkörperabfrage, URL, https://wasser.umweltbundesamt.at/h2odb/stammdaten/igwk.xhtml.